REVIEW

Graphene oxide membranes: The controlling of transport pathways

Pengcheng Su,[a] Fei Wang,[a] Zhanjun Li,[a] Chuyang Y. Tang[b] and Wanbin Li*[a,b]

Graphene oxide (GO) nanosheets with atomic thickness and tunable physicochemical property have been considering as promising nanobuilding blocks for fabrication of separation membranes with impressive performance. There are two kinds of molecular transport channels in laminar GO membranes, interlayer nanochannels formed by adjacent nanosheets and intrinsic defects/pores/edges of GO nanosheets. It has been dmonstrated that the precise controlling of transport pathways at angstrom level, through reduction, molecule/cation cross-linking, intercalation, physical confinement, electric field adjusting, pore creating, and defect sealing, can greatly improve the separation performance of GO membranes. Herein, we first briefly review the fabrication strategies of GO membranes and then comprehensively disscus the merits and mechanisms of controlling transport pathways of GO membranes for liquid separation applications including static diffusion, pressure-driven filtration, and pervaporation.

1. Introduction

As an advanced technology, membrane separation possesses many unique advantages such as low energy consumption, simple operation, and environmental friendliness, relative to conventional distillation, condensation, etc.[1-6] Moreover, membrane separation can be conducted in continuous mode and displays low-cost maintenance. As a semipermeable barrier, membrane allows the passage of desired species and hinders unwanted ones. To achieve highly efficient separation, membranes should have large permeate flux, high selectivity, and excellent stability under various conditions. However, commercial polymeric and inorganic membranes are currently restricted by the well-known trade-off phenomenon between permeability and selectivity.[7-9] Therefore, it is of great importance to develop novel membrane materials with highly permeable and selective performance.

Recently, various two-dimensional (2D) materials, including zeolites,[10-12] metal organic frameworks (MOFs),[13-16] covalent organic frameworks (COFs),[17-19] graphene,[20-22] MXene,[23-25] MoS_2,[26-28] C_3N_4,[29,30] and other nanosheet materials,[31-33] have been employed as attractive building blocks to prepare high-performance separation membranes, due to their unique atomic thickness, easy preparation, capable of functionalization, and micrometer lateral dimensions. The intrinsic nanopores derived from porous structures as well as the controllable nanochannels between stacked nanosheets contribute to precise and fast transport of molecules through 2D membranes. Through delicately tuning nanostructures, precise perforating, and sophisticated controlling nanoscale transport channels, many great progresses about 2D nanosheet membranes for molecular separation, e.g. gas separation, desalination, organic solvent nanofiltration, and pervaporation, have been achieved.[34-36]

Among these 2D materials, graphene, the monolayer of graphite, is constructed by a single atomic sheet of sp^2 hybridized carbon atoms with honeycomb lattice, which receives much attention as membrane materials due to their extraordinary mechanical strength and chemical stability, along with cost-effective production processes and exclusive atomic thickness.[37-40] The perfect monolayer graphene is almost impermeable to gases even including helium because of the high electron density in aromatic rings.[41,42] To open up potential applications of graphene in molecular sieving, nanopores are created in graphene sheets to prepare nanoporous graphene membranes, which show strong mechanical strength, large permeation flux, and high rejection rate in separation application.[43] However, the complex procedures of pore controlling and the strict requirements in fabrication process make the nanoporous graphene membranes difficult to be scaled up for industrial application. Graphene oxide (GO) nanosheets, one of the most important derivatives of graphene, can be cost-effectively synthesized by chemical oxidization, solvent-assisted exfoliation, and electrolytic oxidation of graphite, obtaining a lot of research interests.[44] Different from graphene, GO nanosheets possess large numbers of carboxyl, hydroxyl, epoxy, and carbonyl groups, which provide the potential to delicately control the physicochemical properties of GO nanosheets. For example, the hydrophilic groups make GO nanosheets easily dispersible in aqueous media to form well-dispersed aqueous GO colloids, which provide a facile approach to assemble GO nanosheets into thin laminar membranes. Nair *et al*. conducted the pioneering work of GO membranes and proved that submicrometer-thick

[a] School of Environment and Guangdong Key Laboratory of Environmental Pollution and Health, Jinan University, Guangzhou 511443, P.R. China. E-mail: gandeylin@126.com
[b] Department of Civil Engineering, The University of Hong Kong, Pokfulam, Hong Kong 999077, P. R. China.

GO membranes were impermeable to liquids, vapors, and gases, but permitting unimpeded permeation of water.[20] After that, various GO membranes with well-defined laminar structures assembled by filtration, coating, layer-by-layer (LBL) deposition, etc., have been developed for liquid separation applications.[45]

As known, most GO nanosheets are prepared by strongly oxidation of graphite under acidic conditions, producing highly oxidized and non-oxidized regions in single-layer GO nanosheets. The oxygen-containing functional groups make adjacent GO nanosheets apart from each other, thus generating interlayer galleries in laminar membranes, and also they help water to pass through GO nanosheets in a hydrated state. For the non-oxidized regions, they provide rapid capillary network, which permit correlated water to nearly frictionless flow. In the dry state, GO membranes possess a typical interlayer spacing about 8.0 Å.[46,47] When GO membranes soak into an aqueous solution, the interlayer spacing will be enlarged to more than 13.5 Å, and even to 60−70 Å, due to the adsorption of large amount of water molecules, thus providing larger nanochannels to transport various molecules or ions. However, the enlarged interlayer spacing in water is larger than the diameters of hydrated ions of common salts, leading to a great challenge for GO membranes to achieve high salt rejection (especially for Na^+ and K^+). Moreover, in the permeation process of GO membranes, molecules first enter into the defects/pores/edges in GO nanosheets and then transport through plane-to-plane intergalleries, the appropriate manipulation of intrinsic defects/pores/edges can improve the transport processes.[48] Therefore, it is vital to control the interlayer spacing expansion of GO membranes and regulate their defects/pores/edges for achieving sharp molecular separation. The detailed methods to control the interlayer spacings and defects/pores/edges of GO membranes are discussed in the following sections.

The published reviews about GO membranes mainly focus on summarizing the following aspects: physicochemical properties, preparation approaches, and applications in molecular separation. The latest researches have already proved that the accurate control of molecular transport channels is vital to realize the applications of GO membranes for precise molecular separation.[49-52] However, there is no review to comprehensively summarize the latest approaches and discuss the mechanisms in precisely controlling transport pathways of GO membranes. Therefore, our review aims to discuss the remarkable advances in manipulation of transport pathways including interlayer nanochannels formed by adjacent nanosheet interactions and intrinsic defects/pores/edges of GO nanosheets.

2. Fabrication of GO membranes

As one of the most important 2D materials, GO nanosheets with high aspect ratio structures can be easily assembled into laminar membranes on porous substrates by a series of liquid-phase preparation methods including vacuum/pressure-driven filtration, coating, casting, LBL assembly, and electrophoresis deposition (ED).[53] Vacuum/pressure-driven filtrations are most widely used methods to obtain GO membranes with porous substrates. The thicknesses of GO membranes can be controlled by changing the introduced amount of GO suspension straightforwardly. Beside filtration methods, coating or casting approaches such as spin-coating, spray-coating, and drop-casting have been employed for rapid assembly of GO membranes as well. The interfacial adhesion between substrates and GO nanosheets can be improved by hydrogen bonding, electrostatic interaction, and covalent bonding through surface modification.[54] GO membranes can also be prepared by LBL assembly of GO nanosheets. By changing the number of deposition cycles, LBL strategy can adjust the thickness of GO membranes at molecular level. Recently, ED method is further developed for preparation of GO membranes. In this section, we briefly summarize some typical fabrication methods of well-defined laminar GO membranes and discuss their unique advantages in practical applications.

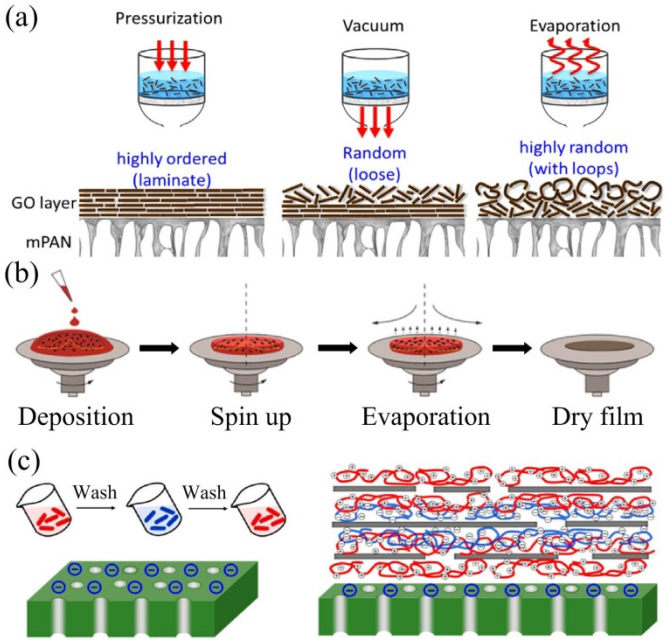

Fig. 1. (a) Schematic diagram of GO membranes assembled by pressure-driven filtration, vacuum-driven filtration, and evaporation methods. Reproduced with permission from ref. 61. Copyright 2015, Elsevier. (b) Fabrication of ultrathin GO membranes through spin coating method. Reproduced with permission from ref. 62. Copyright 2016, American Chemical Society. (c) Scheme of the synthesis route for PE@ArGO membranes by LBL assembly. Reproduced with permission from ref. 70. Copyright 2017, American Chemical Society.

2.1. Vacuum/pressure-driven filtration

Vacuum/pressure-driven filtrations are most widely adopted approaches for large-scale preparation of laminar GO membranes with porous polymer/inorganic substrates.[55-57] Stronger hydrogen bonding and van der Waals attractive forces between the adjacent GO nanosheets endow GO membranes with ordered and compact structures. The guest molecules pass through stacked nanochannels between adjacent nanosheets in layered GO membranes to achieve efficient separation. The thickness of GO membranes can be precisely tuned by changing the introduced amount of GO suspension. Yang *et al*. reported the fabrication of ultrathin GO membranes (down to ~10 nm) by

vacuum filtering aqueous GO solutions through anodisc alumina substrates for ultrafast and efficient solvent permeation.[58] The thickness of membranes could be delicately regulated by filtrating different volumes of GO suspension. It should be noted, when the introduced GO amount is too large, the required fabrication time will sharply increase once the deposited thickness of the GO membranes reach at several micrometers.[59] On the other hand, the non-uniform GO membranes with serious defects may be produced if the inadequate GO suspension was introduced. Therefore, the added amount of GO suspension with concentration of tens to hundreds mg L^{-1} for preparation of GO membranes should be reasonable chose.

Fabrication conditions such as deposition rate and driving force have great effects on the nanostructures and permeation characteristics of GO membranes. Xu *et al*. deposited GO nanosheets at different rates by vacuum-assisted filtration to regulate the interlayer nanostructures of lamellar GO membranes and investigated the process-structure-performance relationship of membranes.[60] The prepared lamellar GO membranes assembled by slow deposition of GO nanosheets showed 2.5−4 times higher pure water permeation flux and obviously improved salt rejection than that of the membranes fabricated at fast rate. When the lamellar GO membranes were deposited at slow rate, the oxygen-containing groups on neighboring GO nanosheets tended to self-assemble with each other to approach the thermodynamically favoured interlayer structures, thus producing fast water transport nanochannels. On the contrary, the less favorable interlayer structures would be formed at fast deposition rate, resulting in the sharply reduced water permeation. The driving forces of filtration show significant effect on the structures and performances of lamellar GO membranes. Tsou *et al*. prepared the GO membranes on modified polyacrylonitrile (mPAN) supports by three different approaches (pressure, vacuum, and evaporation-assisted self-assembly) to investigate the influence of assembly procedures on the microstructures and performances of GO membranes (Fig. 1a).[61] For the filtration under vacuum, the loose GO layers were formed on the surfaces of the GO membranes due to the increased cake resistances and decreased vacuum driving forces. When GO was deposited by evaporation at controlled humidity, the upward driving force combined with the vaporizing liquid led to the GO layers in highly random order. In comparison with the abovementioned two assembly methods, the pressure-assisted filtration induced by the constant-pressure driving forces with liquid down-flow direction endowed the GO membranes with more ordered laminate structures, higher hydrophilic characteristics, and better performance in pervaporation dehydration.

2.2. Coating and casting

Besides filtration, coating and casting approaches, such as spin-coating, spray-coating, dip-coating, and drop-casting, have been employed for rapid assembly of GO membranes as well. The substrates with good affinity and oppositely charged property to GO nanosheets and possessing abundant functional groups to react with GO nanosheets, may be suitable for GO coating, because these features will greatly improve the uniformity, continuity, and stability of GO membranes. For spin-coating method, the homogeneous GO solution is spread out uniformly on the support under centrifugal force, leading to the formation of an ultrathin and laminar GO membrane. Chi *et al*. employed the freeze-thaw exfoliation method to produce large GO nanosheets and then successfully obtained the ultrathin GO membranes with the thickness of 20 nm through spin coating method (Fig. 1b).[62] It should be noted that the delicate control of deposition speed and solvent (water) evaporation rate is critical for forming high-quality GO membranes. Faster deposition may cause the overflow of GO solution in spin coating process, while faster evaporation will produce inhomogeneous distribution of GO nanosheets. In order to improve the large-scale production ability of GO membranes, spray-coating technology was developed. Fathizadeh *et al*. prepared the large area GO nanofiltration membranes (15×15 cm^2) on the modified polyacrylonitrile supports, using simple, fast, and scalable spray printing technology by commercial printer.[63] Wang *et al*. reported the preparation of heterostructured polydimethylsiloxane (PDMS)@GO membranes by spray coating GO dispersion and PDMS solution.[64] The adopted spray-coating preparation method with simple, scalable, and low-energy features possesses great potential in future industrial applications. Recently, various casting technologies were adopted to large-scale produce GO membranes. Akbari *et al*. reported the casting of GO dispersion on porous nylon substrates to produce large area GO membranes (13×14 cm^2) in less than 5 s.[65] Zhong *et al*. applied continuous centrifugal casting in fabricating meter-scale free-standing GO films with highly aligned and compact structures.[66]

It is noticeable that the contact way of substrate surface to GO solution plays a critical role in determining the laminate structures of the GO membranes prepared by coating method. When the substrate surface first contacts to the air-liquid interface of GO solution then followed by spin-coating, the initial electrostatic repulsion forces between the adjacent GO edges will cause a relatively heterogeneous GO deposition. On the contrary, when GO solution is dropped directly onto the substrate during spin-coating process, a highly ordered laminar GO structures will be produced, because the capillary interactions between faces of GO nanosheets overcome the electrostatic repulsions between GO edges.[67]

2.3. Layer-by-layer (LBL) assembly

Owing to its laminar structures and charged oxygen-containing functional groups, GO nanosheet can be used to prepare laminar GO membranes by LBL assembly method. By changing the number of deposition cycles, LBL strategy can adjust the thickness of GO membranes at molecular level.[68] Fabrication of thin GO membranes by LBL assembly method is usually conducted by alternatively depositing polyelectrolytes and GO nanosheets through electrostatic interactions, hydrogen bond or other multiple molecular interactions (hydrophobic interactions, covalent bond, and coordination interactions, etc.). Compared with the coating and casting performed by loading GO nanosheets on substrates, the LBL assembly mainly involves the layer-by-layer construction process and the design of mutual

interactions between different layers. Zhao *et al*. prepared the GO-based ultrathin hybrid membranes with thickness less than 115 nm by LBL self-assembly through alternately depositing Gelatin (GE) and GO on hydrolyzed polyacrylonitrile supports.[69] As a positively charged polyelectrolyte, GE interacted with GO in the self-assembly process through various types of forces including electrostatic attraction, hydrogen bond, and hydrophobic interaction, thus leading to efficient LBL self-assembly of GE and GO.

To further improve the nanostructures and separation performances of the GO membranes prepared by LBL assembly method, the used GO nanosheets need to be functionalized and anchored with polyelectrolyte. Song *et al*. employed ethylenediamine (EDA) molecules to modify GO nanosheets, which were then anchored by poly(allylamine hydrochloride) (PAH) to enhance the surface charge density.[70] As shown in Fig. 1c, PAH@ArGO nanosheets with positive charge and PSS@GO nanosheets with negative charge were alternately deposited on the polycarbonate substrates by LBL assembly method, producing the polyelectrolyte intercalated amine rGO membranes (PE@ArGO membranes). The prepared PE@ArGO membranes, with rejection layer about 160 nm in thickness, possessed high density positive/negative charge gated ion transport nanochannels and excellent salt rejection governed by Donnan charge exclusion. The electrostatic LBL assembly process is based on the interaction of oppositely charged GO nanosheets, which will be easily influenced by the assembly pH. The thickness, morphology, charge density, and internal structure of the assembled GO membranes can be precisely tuned by changing the pH values in the GO suspensions. The GO membranes assembled in alkaline pH condition are relatively thicker and rougher, due to the random layer conformation of 2D charged GO nanosheets. Moreover, when the GO membranes are assembled in the acidic pH condition, the produced charge compensation between weakly charged GO^- nanosheets and highly protonated GO^+ nanosheets will also lead to a thick GO film growth. On the contrary, a moderate growth of GO layers can be obtained in neutral pH, in which GO^+ and GO^- nanosheets show the homogenous charge distribution and strong binding forces between the charged and planar GO layers, promoting the formation of dense and thin GO membranes.[71,72] However, the inherent physicochemical features of GO membranes may be disturbed when the excessive amount of functionalized molecules or polymers were introduced.

2.4. Electrophoresis deposition

Electrophoresis deposition (ED) is a well-developed nanoscale assembly technology in which charged colloids suspended in liquid solution will migrate under the electric field and then deposit onto the surface of electrode. Due to the advantages of high deposition rate, easy magnification, precise controlling in the thickness, and low production cost, ED has been widely applied in preparing thin films from charged colloidal suspensions.[73] For GO nanosheet, the highly hydrophilic character and existence of easily deprotonated functional groups endow it with excellent dispersion in water and negative charges, which are beneficial for preparation of GO membranes by ED method. An *et al*. proved that ED method could be utilized to deposit GO films on electrically conductive substrates with the deposition time of 1-10 min.[74] During the ED process, the oxygen functional groups were significantly removed due to the reduction of GO. It should be noted that the suspension pH and deposition voltage play a critical role in determining the structures of GO membranes. Hasan *et al*. found that cathodic deposition of GO would occur in the low pH suspension and high voltage, which resulted in a gradual change in the colloids from negative to positive charge due to the adsorption of protons released by the electrolysis of water. The shift in the charges of colloids triggered the formation of porous brick structures of GO membranes, because the decrease in electrostatic repulsion between GO sheets produced multilayered aggregates.[75] By using large-area electrode, ED method can also be employed in large-scale production of GO membrane. Wang *et al*. reported the fabrication of large-area rGO membrane with the size of 10×10 cm^2 on the stainless steel (SS) electrodes by ED technology.[76] In general, ED technology shows great prospect in highly efficient preparation of GO membranes.

3. Controlling of transport pathways

For laminar GO membranes, there are two kinds of molecular transport channels: (1) interlayer nanochannels formed by adjacent nanosheets and (2) intrinsic defects/pores/edges of GO nanosheets.[77] The precise controlling in the transport channels of GO membranes possesses significant effect on selectively transporting molecules or ions. In the mass transfer process of GO membranes, molecules first enter into the defects/pores/edges in GO nanosheets and then transport through plane-to-plane channels. For the ultrathin membranes with mono-layered and few-layered GO nanosheets, the intrinsic defects and pores are main transport pathways and play the critical roles for size exclusion. For the membranes with relatively thicker selective layers, the much longer interlayer nanochannels between the adjacent GO nanosheets offer the selectivity and determine the permeation. The microstructures of the interlayer nanochannels greatly influence the selective transport of molecules. The size of channels lead to the behaviors of molecular sieving, and the functional hydrophilic hydroxyl, carboxyl, and epoxide groups on GO nanosheets affect the transport process of the molecules through GO membranes, via adsorbing water molecules and providing negatively charged effects for Donan exclusion.[78,79] The mass transfer mechanism of GO membranes is largely dependent on synergistic effects of defects/pores/edges of nanosheets, 2D interlayer channels between adjacent nanosheets, and functional groups on GO.

Controlling the transport channels of GO membranes at angstrom level is vital for sharp molecular separation. The interlayer spacing of GO membranes has been proven to possess significant effect on molecular transport efficiency. It can be tuned by chemical and physical methods. For chemical tuning, some functional molecules/cations are introduced to cross-linking GO membranes for immobilizing the interlayer spacing. By using different cations, the accurately controlled d-spacing can be obtained for ion sieving in static diffusion.[50] However, the

intrinsic geometry of molecules/cations between GO nanosheets makes this approach difficult to produce small and robust enough interlayer channels for pressure-driven membrane separation. Beside chemical strategies, physical methods, such as intercalation by nanomaterials and regulation by external pressure, have been proved with good feasibility to tune the interlayer spacing.[51] Moreover, researchers also apply chemical etching, high temperature reduction, and combustion synthesis to generate intrinsic defects and pores in GO nanosheets.[80] Defects, pores, and edges of GO membranes can provide transport pathways for improving performance. In this section, controlling methods of transport pathways in GO membranes are divided into the following categories: chemical or physical methods to precisely control the interlayer spacings of adjacent GO nanosheets, and manipulating the intrinsic defects or pores in GO nanosheets.

3.1. Controlling interlayer spacing by chemical methods

As mentioned above, precise manipulation of interlayer spacing possesses significant effect on molecular transport efficiency. During liquid-based separation, laminar GO membranes often become swollen and their interlayer spacing will be enlarged, due to the capillary suction for the liquid and solution. This phenomenon will cause the poor rejection for salts and small solutes, and even the gradual dissociation of GO membranes.[81] Therefore, it has great scientific and practical interests to control the transport pathways and improve the stability of GO membranes. There are about several chemical methods listed below to control the interlayer spacing of GO nanosheets: 1) reduction; 2) cross-linking; 3) cation-controlling; 4) *in situ* intercalation.

3.1.1. Reduction

Since the tighter GO membranes are actually more suitable for small molecule sieving, narrowing the 2D interlayer spacing of GO membranes is attractive. Chemical reduction of GO membranes has been one of most popular method to narrow the interlayer nanochannels of GO membranes. Various reduction methods, including chemical reduction,[82] thermal treatment,[83,84] ultraviolet irradiation,[85] and ED[86] have been proposed for fabrication of rGO membranes. As shown in Fig. 2a, the freestanding ultrathin rGO membranes with thicknesses down to 20 nm were prepared through chemical reduction of the GO membranes by hydriodic acid (HI) vapor and water-assisted delamination.[87] This chemical reduction strategy by HI steam was relatively facile and efficient. After HI reduction, the d-spacing decreased from 8.7 Å of the pristine GO membranes to 3.5 Å of the rGO membranes, due to the removal of oxygen containing groups on GO surface. It should be noted that the vapor exposure time plays a critical role in reduction degree of GO laminates. Yang *et al.* investigated the reduction degree of GO membranes by varying exposure time to HI vapor for precisely tuning the size of GO nanochannels in sub-nanometer range.[88] As the HI vapor exposure time increased from 0 to 5 min, GO membranes would suffer higher degree reduction with the increased C/O element ratios on their laminates, and the interlayer distance of laminar GO membranes was gradually declined from 11.5 to 3.7 Å under wet condition.

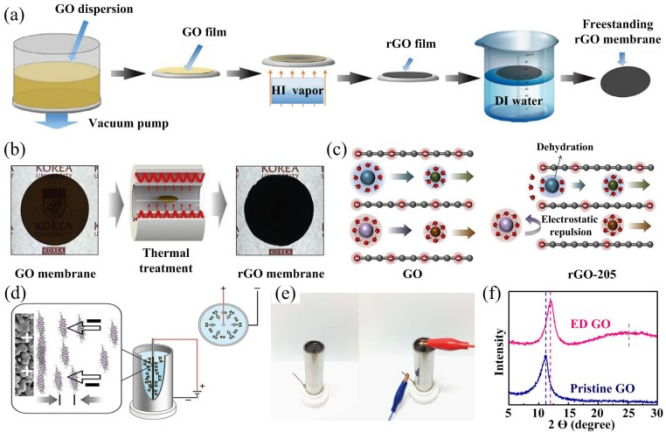

Fig. 2. (a) Schematic diagrams of fabrication process of freestanding rGO membranes by HI vapor reduction. Reproduced with permission from ref. 87. Copyright 2015, John Wiley and Sons. (b) Preparation process of rGO membranes by thermal treatment. (c) Illustration of ion sieving mechanism of GO membranes and rGO-205 membranes. Reproduced with permission from ref. 89. Copyright 2019, Elsevier. (d) Schematic synthesis process of ED-GO membranes by ED. (e) Photos of the electrolytic cell for GO ED. (f) XRD pattern of pristine GO and ED-GO layers. Reproduced with permission from ref. 86. Copyright 2017, Springer Nature.

Although chemical reduction of GO membranes through chemical reagents can be completed by only few minutes, the usage of strong acid vapor is not so much environmental friendly. In contrast, a more mild reduction can be achieved by thermal treatment. Kim *et al.* prepared rGO membranes with different contents of oxygen functional groups through thermal treatment (Fig. 2b).[89] To investigate the influence of oxygen containing groups and interlayer spacings on the ion and water permeation, GO membranes were thermally reduced at different temperatures (175, 190, 205, and 220 °C). As the temperature increased from 175 to 220 °C, the contents of oxygen functional groups on GO surfaces gradually decreased, coupled with the interlayer spacing declined from 8.0 Å of the pristine GO membranes to 5.0 Å of the GO membranes reduced at 220 °C. Due to the existence of negatively charged oxygen functional groups on the GO surface, the movement of multivalent anions through 2D nanochannels of the rGO membranes was limited by electrostatic repulsion (Fig. 2c).

As a well-developed, environmentally friendly, and economical technology, ED method can also be applied in reduction of GO membranes. As shown in Fig. 2d, the ultrathin GO layers were assembled on the porous stainless steel hollow fibers (PSSHFs) by ED technology. When applying a DC voltage on circular electric field (Fig. 2e), the negative charged GO nanosheets were partially reduced by the cathode, and then driven by the electrostatic interaction to deposit onto the surface of the PSSHF substrates. In the ED process, the thickness of the ED-GO membranes was nearly linear dependent on the ED time, and the oxygen functional groups on GO sheets were selectively reduced, producing the narrowed 2D nanochannels between stacked GO layers. XRD results proved that the interplanar spacing decreased from 8.0 Å of pristine GO to 7.3 Å of ED-GO

(Fig. 2f).[86] The ED method for deposition of ultrathin, defect-free, and compact GO layers was proved to be facile and fast, in which the ED-GO membranes can be fabricated by only 35 s.

It is worth noting that the interlayer distance of GO nanosheets may be enlarged by chemical reduction, when small molecules cross-linkers are introduced and inserted between the adjacent rGO sheets. Thebo *et al*. prepared the laminar rGO membranes with extended interlayer distance by using theanine amino acid (TH) and tannic acid (TA) as reducing agents and cross-linkers.[90] Compared with the GO membranes with the interlayer distance of 7.6 Å, the prepared rGO–TA and rGO–TH membranes showed larger interlayer distance of 9.9 Å and 8.5 Å, respectively. This phenomenon was induced by the intercalation of TA or TH among the adjacent rGO nanosheets. The greatly increased graphitic domains were produced owning to the removal of oxygen containing groups, which was beneficial for rapid water transport by nearly frictionless flow. The strong π–π attraction in the normal domains along with the strong covalently bonding between rGO nanosheets and TA/TH molecules greatly improved the stability of rGO–TA and rGO–TH membranes in aqueous solutions, with no degradation even after 90 days. Although much progress has been obtained in tuning interlayer distance of GO laminates by chemical reduction, the obvious decrease of oxygen functional groups in GO membranes after reduction may lead to the low water permeation.

3.1.2. Cross-linking

As an early developed method, chemical covalent cross-linking GO membranes are usually carried out by intercalation of specific small molecules or polymers capable of reacting with oxygen-containing functional groups on GO, which has been proved to be simple and effective in adjusting the interlayer spacing of laminar GO membranes and limiting the mobility of GO sheets in aqueous solutions. Until now, the typically used cross-linkers can be divided into two categories according to the difference in molecular weights. 1) Small molecule cross-linkers such as amines,[91-95] diisocyanate,[96,97] dicarboxylic acid,[98] sulfosuccinic acid,[99] urea,[100] fullerenes,[101] and thiourea.[102] As shown in Fig. 3a, Hung *et al*. reported the cross-linking of GO by diamine monomers to fabricate GO composite membranes through pressure-assisted filtration technique.[91] Three kinds of diamine monomers including ethylenediamine (EDA), butylenediamine (BDA), and p-phenylenediamine (PPD) were selected in the test. After reaction, the diamine monomers chemically bonded to the GO surfaces and cross-linked GO nanosheets. XRD results indicated that the d-spacing of these membranes in the wet state varied from 13.1 Å (unmodified GO layer) to 9.3 Å (EDA-cross-linked GO layers). Moreover, in contrast with the hydrogen bonds and π−π interactions between the unmodified GO layers, the C−N covalent bonds produced at the cross-linked GO layers could effectively suppress the stretching of the interlayer spacing in solution, which helped to improve the stability of GO membranes during long-term operation.

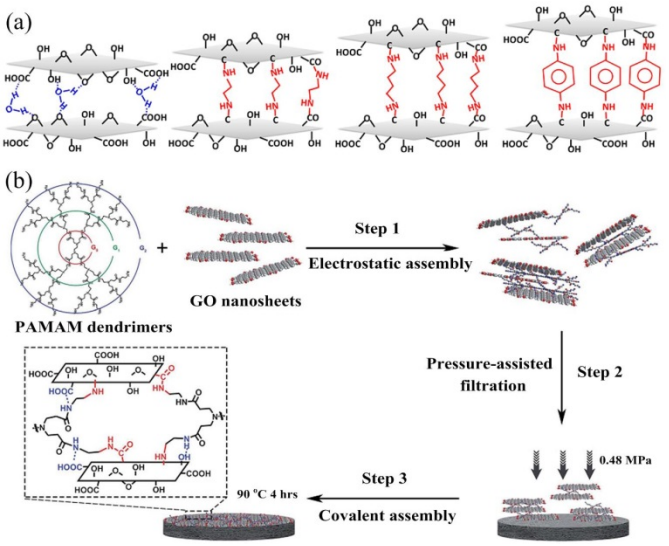

Fig. 3. (a) Structures of GO, GO-EDA, GO-BDA, and GO-PPD membranes. Reproduced with permission from ref. 91. Copyright 2014, American Chemical Society. (b) Synthetic diagram of GO-PAMAM membranes. Reproduced with permission from ref. 109. Copyright 2019, Royal Society of Chemistry.

In order to achieve highly cross-linking, large amount of small molecule cross-linkers are used to react with the hydroxyl, carboxyl, or epoxy groups on the GO surface during membrane preparation, which will lead to the considerable occupancy of 2D nanochannels. Furthermore, a lot of oxygen-containing sites are replaced or dominated by other groups in cross-linking reaction, which weaken the interaction forces between water molecules and GO.[103] 2) Polymer cross-linkers such as polyethylenimine (PEI),[104-107] boronic acid polymer (BA),[108] dendrimers,[109] and poly(ethylene glycol) (PEG).[110,111] Generally, polymer cross-linkers possess abundant functional groups and can easily anchor GO nanosheets at a relative low adding amount, producing a dense GO/polymer composite structure. After intercalation by polymer cross-linkers, the interlayer spacing of GO nanosheets can be precisely controlled among a broad range from subnanometer to several nanometers, owing to the linear or randomly entangled conformation of polymer chains.[112,113] As shown in Fig. 3b, primary amine-terminated polyamidoamine (PAMAM) dendrimers with regularly branched structures and multiple amine groups were selected as cross-linkers to control the interlayer spacing of GO membranes. After cross-linking, the interlayer spacing of the GO membranes can be precisely controlled in the range of 4.3–7.6 Å in the wet state, owing to the robust covalent cross-linking between adjacent GO nanosheets and the compact structures of the dendrimers.[109] The chemical cross-linking by polymers on adjacent GO nanosheets can precisely tune the interlayer spacing and improve the stability of GO membranes in water. However, the cross-linked large polymer backbones between GO nanosheets may greatly occupy the free volume in 2D channels, thus producing barrier for molecule transport.

Although covalent cross-linking of GO membranes has achieved much progress, it still faces the problems in

considerable occupancy of 2D nanochannels and weakened interaction forces of GO for water molecules, which may produce barriers for water entering and subsequent transport. Different from covalent cross-linking method, non-covalent cross-linking is formed by π–π, electrostatic, and hydrogen bonding interactions, which will not dominate the oxygen-containing functional groups on GO.[114,115] Ran *et al*. improved the stability of GO membranes by intercalating ionic polymers into adjacent GO nanosheets, which was connected by non-covalent cross-linking interactions.[103] Imidazolium functionalized brominated poly(2,6-dimethyl-1,4-phenylene oxide) (Im-PPO) and sulfonated poly(2,6-dimethyl-1,4-phenylene oxide) (S-PPO) were selected as cross-linkers, which connected neighboring GO nanosheets by non-covalent π–π and electrostatic interactions, non-covalent π–π and hydrogen bonding interactions, respectively. This non-covalent cross-linking method is tested to be effective in improving the stability of the GO membranes in water, with no degradation after 90 days. As shown in Fig. 4, the GO nanosheets were modified by solvent green (SG) through the strong π-π stacking interactions and then assembled into the laminar SG@GO membranes on the PDA-modified tubular ceramic substrates. After the non-covalent cross-linking, the interlayer spacings between GO nanosheets could be tuned from 7.7 to 8.4 Å.[116]

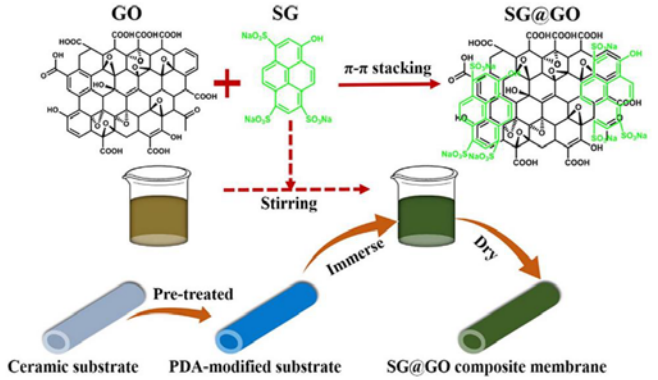

Fig. 4. Scheme of non-covalent cross-linking GO nanosheets by π–π stacking interactions and preparation of SG@GO membranes on tubular ceramic substrates. Reproduced with permission from ref. 116. Copyright 2017, Elsevier.

Chemical modification of GO nanosheets can be an effective approach to delicately tune the nanostructures, functionalities, and interlayer spacings of GO membranes. The reported chemical modification methods mainly include the flowing categories such as graft of functional polymers or molecules,[117-119] nitrogen doping,[120] and biomolecules immobilization.[121] Li *et al*. reported the preparation of polysulfone (PSf)-grafted GO nanosheets (GO-g-PSf) by nucleophilic substitution reaction between hydroxyl groups on GO and chloromethyl groups on chloromethylated PSf. The graft of PSf on GO nanosheets not only improved the structural stability of the GO-g-PSf membranes, but also enlarged the interlayer spacing of adjacent GO nanosheets due to the large extent physical entanglement of PSf chains.[122] As shown in Fig. 5, nitrogen-doped graphene (NG) was prepared by simple hydrothermal treatment with ammonia hydroxide (NH_4OH) and then assembled into NG membranes by vacuum filtration. The obtained NG nanosheets, possessing different N contents and nitrogen-bonding configurations through changing the doping reaction time, produced narrower interlayer spacing and more-polarized surface than the pristine GO. After soaking in water, the NG membranes could maintain the interlayer spacing stationary at around 3.6 Å, while the interlayer spacing of the GO membranes would increase from 9.7 Å to 10.8 Å.[120]

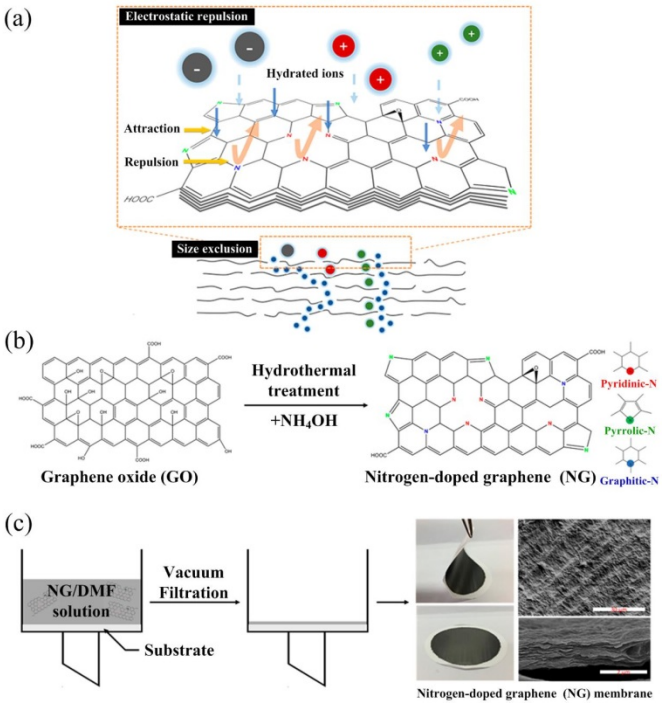

Fig. 5. (a) Scheme of ion sieving through NG membranes by the combined effect of electrostatic interactions and size exclusion. (b) Fabrication process of nitrogen-doped graphene (NG) from GO. (c) Preparation process of NG membranes, digital photos and SEM images of NG membranes on PTFE substrate. Reproduced with permission from ref. 120. Copyright 2018, American Chemical Society.

3.1.3. Cation-controlling

Cation-controlling method, using monovalent, bivalent, and tervalent cations,[123,124] can tune the interlayer spacing sufficiently to exclude small ions and suppress the tendency of GO membranes to swell when immersed in water. Chen *et al*. reported that metal cations (K^+, Na^+, Ca^{2+}, Li^+, and Mg^{2+}) themselves could control the interlayer spacing of GO membranes at sizes as small as a nanometre and the variable range of this spacing could be precisely tuned at one ångström (Fig. 6a and b).[50] As shown in Fig. 6c, the interlayer spacings of the GO membranes immersed in pure water or in various salt solutions for one hour, could be controlled in the order of $MgCl_2$> LiCl> $CaCl_2$> pure water>NaCl>KCl, with the largest value of 13.6 Å in $MgCl_2$ solution and the smallest value of 11.4 Å in KCl solution. When the GO membranes were first immersed in KCl solution and then soaked them in various salt solutions (NaCl, $CaCl_2$, LiCl or $MgCl_2$), the corresponding interlayer spacings were almost consistent with that of the GO membranes only immersed in KCl solution (Fig. 6d), which was resulted from the

stable and effective control of the interlayer spacing at about 11 Å by K^+, thus leading to the exclusion of other cations. Molecular simulation proved that the fixing of interlayer distances by cations was mainly by the strong noncovalent cation–π interaction between the hydrated cations and the aromatic rings on GO sheets, as well as the interaction between the hydrated cations and the oxygen functional groups on GO sheets.

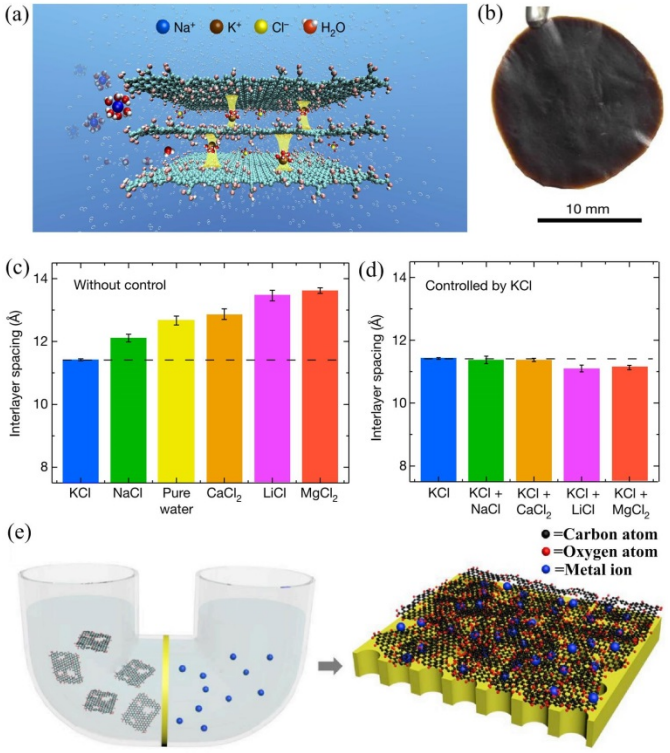

Fig. 6. (a) Schematic diagrams of how K^+ ions in GO membranes control the interlayer spacing. (b) Photo of a freestanding GO membrane. (c) Interlayer spacing of GO membranes immersed in pure water or in various salt solutions. (d) Interlayer spacing of GO membranes first soaked in KCl solution, followed by immersing in various salt solutions. Reproduced with permission from ref. 50. Copyright 2017, Springer Nature. (e) Scheme of cation-controlled GO membranes prepared by contra-diffusion method. Reproduced with permission from ref. 126. Copyright 2020, Elsevier.

Besides the monovalent and bivalent cations, tervalent cations can also be employed to control the interlayer distance of GO membranes. Liu *et al*. used two trivalent cations (Al^{3+} and Fe^{3+}) as cross-linking agents to assemble GO nanosheets on the PVDF supports.[125] Al^{3+} and Fe^{3+} could greatly enhance the bonding strength between GO nanosheets through electrostatic interactions and coordination bonds, thereby improving the stability of the GO membranes with the integral structure in water, sodium salt (SA), and bovine serum albumin (BSA) solutions for at least two weeks. The pristine interlayer distance of GO nanosheets (8.0 Å) could be expanded to 8.6–9.5 Å through inserting Al^{3+} or Fe^{3+} ion. It should be noted that the cation-controlling can also be realized by contra-diffusion method. As shown in Fig. 6e, the GO aqueous solution and the cation aqueous solution were separately placed on both sides of the support. The metal cations diffused into the GO solution and cross-linked the GO nanosheets to assemble into laminar GO films. The strong cation-π and electrostatic forces between cations and GO nanosheets leaded to a fast deposition with only 5 min. Various cations (Na^+, K^+, Mg^{2+}, Ca^{2+}, and Fe^{3+}) can be employed as cross-linkers to control the interlayer spacing of GO films for achieving high nanofiltration performances.[126]

3.1.4. *In situ* intercalation

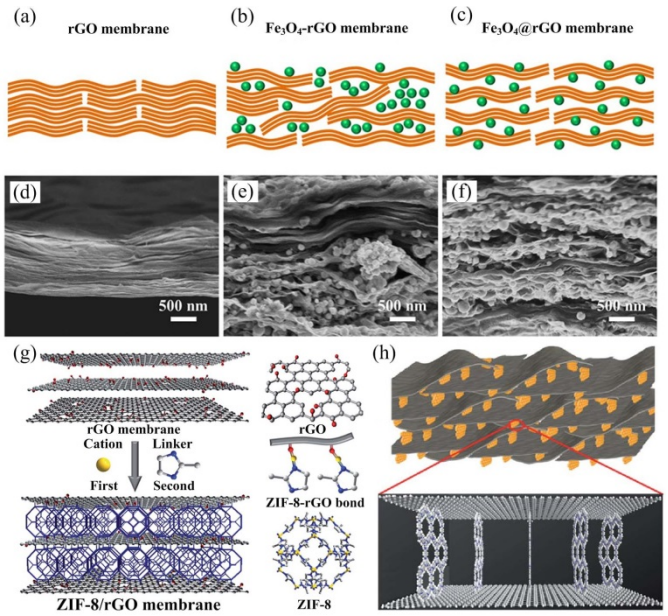

Fig. 7. (a-f) Schematic diagrams and cross-sectional SEM images of (a,d) rGO, (b,e) Fe_3O_4-rGO, and (c,f) Fe_3O_4@rGO membranes. Reproduced with permission from ref. 131. Copyright 2017, John Wiley and Sons. (g) Fabrication process of ZIF-8/rGO membranes by *in situ* crystallization. Reproduced with permission from ref. 130. Copyright 2016, Royal Society of Chemistry. (h) Schematic illustration of GO/v-COF@GO membranes. Reproduced with permission from ref. 139. Copyright 2019, Royal Society of Chemistry.

Recently, *in situ* intercalation method, employing solvothermal reaction to directly produce robust spacers in adjacent 2D GO channels, is used to prepare GO membranes. In contrast with the membranes fabricated by filtration of GO solutions mixed with nanoparticles or nanosheets, the *in situ* intercalated GO membranes possess well-packed structures and uniform transport channels, which are beneficial to improve molecular permeation and precise sieving. Until now, various *in situ* intercalated materials with diverse configurations such as nanorods,[127] nanoparticles,[128,129] and nanosheets[130] have been widely developed. Zhang *et al*. prepared of Fe_3O_4@rGO nanosheets by simple *in situ* solvothermal synthesis and then used it as building blocks to assemble into the laminar membranes on inner surface of ceramic tubes.[131] In Fig. 7a,d, the original rGO membranes without intercalation displayed compacted laminar structure. The Fe_3O_4-rGO membranes fabricated by mixing Fe_3O_4 nanoparticles with rGO dispersion as filtration solutions, appeared uneven intercalation and obvious agglomeration of Fe_3O_4 nanoparticles (Fig. 7b,e), leading to the

disruption of laminar architectures and unselective defects. In contrast, the Fe_3O_4@rGO membranes displayed well-packed layer-by-layer structures consisting of Fe_3O_4@rGO nanosheets, in which the Fe_3O_4 nanoparticles were uniformly intercalated into the adjacent rGO sheets (Fig. 7c,f). Except from the commonly used solvothermal synthesis, atomic layer deposition (ALD) technology has also been applied in the *in situ* intercalation of GO nanosheets. Lam *et al*. reported the preparation of ZnO on the layered GO membranes by 50 cycles ALD growth using diethylzinc and H_2O as precursors.[132] The impregnated Zn healed defects within GO and caused the reduction of intersheet spacing, limiting the transport of organic vapors through the ZnGO membranes.

Compared with the metal oxide nanoparticles, MOFs possess large surface areas and high porosities.[133-135] These features are beneficial for the fast molecular transport through plane-plane nanochannels, when MOFs are intercalated into the adjacent GO nanosheets. Our group reported the fabrication of ZIF-8 nanosheets by simple *in situ* crystallization between GO layers (Fig. 7g), which relied on the polar oxygen groups, extended interlayer spacing in hydrated state, and electronegativity of rGO.[130] The inserted ultrathin ZIF-8 nanosheets were strongly anchored and bolstered up the rGO by coordination bonds, producing uniform and fast nanochannels among neighboring rGO sheets. The permeability of the MOF/rGO membranes can be tuned by introduction of different MOFs with diverse chemical properties and pore sizes (ZIF-7, CuBTC, and MIL-100). Moreover, our group further developed novel interfacial contra-diffusion method to *in situ* embed ZIF-8 into rGO for preparing the ultrathin and uniform ZIF-8/rGO membranes with the thickness of ~150 nm.[136] Beside 2D MOF nanosheets, MOF nanoparticles such as ZIF-8 can also be prepared on the surface of GO nanosheets by *in situ* growth to obtain ZIF-8@GO laminates.[137]

As a kind of porous organic material, COFs possess many unique features such as superior stability, large void spaces, and high accessible surface area.[138] Due to the synthetic versatility, COFs can be endowed with various functional groups such as amino groups, which can be used to covalently connect COFs with adjacent GO nanosheets by reacting with the oxygen containing groups on GO. The intercalated COFs provide an extra passport to improve molecule penetration. All these features make COFs become excellent candidates acting as interlayer spacers for GO membranes. As shown in Fig. 7h, 2D COF nanosheets were employed as intercalation materials grown on GO nanosheets. The anchored amino monomers on GO surfaces were used as nucleation sites to vertically grow 2D COF nanosheets by Schiff-base reaction between amino monomers and aldehyde monomers. After that, the nanoheterojunctions (v-COF@GO) were intercalated into neighboring GO nanosheets by vacuum-assisted filtration, increasing the interlayer spacing from 8.1 Å of the GO membranes to 42.2 nm of the GO/v-COF@GO membranes.[139] Zhang *et al*. also reported the *in situ* growth of COF-1 on the surface of GO nanosheets to synthesize the GO/COF-1 nanocomposites. The embedded COF-1 in the interlayer of GO, with size of 1.5 nm, enlarged the inner spacing of GO, contributing to the fast water molecules pass through the GO/COF-1 nanocomposites.[140]

3.2. Controlling interlayer spacing by physical methods

Although much progress has been obtained in controlling the interlayer transport pathways by chemical methods, the intrinsic geometry of molecules/cations between GO nanosheets makes these approaches difficult to form small and robust enough interlayer channels for achieving the high efficiency desalination in pressure-driven separation process. Apart from chemical strategies, many physical methods such as physical fixation and external pressure regulation, have been proved with good feasibility to accurately restrain the out-of-plane swelling and tune the interlayer spacing of GO laminates, leading to the ultrafast water permeations and high rejections for various salts.[51] In this section, we summarize the latest progresses in delicately tuning transport pathways of laminar GO membranes through physical methods and classify them into three categories: physical intercalation, physical confinement, and electric field controlling.

3.2.1. Physical intercalation

The GO hybrid membranes fabricated by intercalating pre-fabricated materials with various dimensions including 0D nanoparticles and dots, 1D nanowires and nanotubes, and 2D nanosheets into adjacent GO nanosheets, have been successfully obtained with extraordinary separation performance.[141-144] This simple and effective physical intercalation strategy can not only precisely expand the interlayer spacing of GO nanosheets, but also change the hydrophilicity, zeta potential, morphology, thickness, and roughness of the prepared GO membranes. According to the difference in composition, the intercalation materials can be divided into three classes: organic, inorganic, and hybrid materials.

Many organic materials such as carbon dots,[145] GO quantum dots,[146,147] carbon nanotubes (CNTs),[148-150] C_3N_4 nanosheets,[151] rGO,[152] and COFs[153,154] have been developed and inserted into GO nanosheets to prepare GO hybrid membranes with controlled interlayer distance. Morelos-Gomez *et al*. fabricated the hybrid GO membranes through spray coating the mixed aqueous solution contained GO and few-layered graphene (FLG) nanosheets on PSf supports (Fig. 8a).[54] To improve the mechanical robustness of the GO membranes, the PSf supports were coated by polyvinyl alcohol (PVA) as interfacial adhesive layers along with thermal treatment and Ca^{2+} cross-linking. In the intense cross-flow permeation test, the membranes with PVA adhesive layers showed excellent long-term stability with constant performance for up to 120 h. The FLG structures partially covered by deoxycholate (DOC), produced fast water transport nanochannels adjacent to the edges of the FLG. The presence of DOC in the prepared GO/FLG membranes enhanced NaCl rejection (~85%), and resulted in better chlorine resistance than the pure GO membranes. Musielak *et al*. reported the preparation of the stable GO/CNTs membranes by noncovalent interaction between the oxidized CNTs and GO nanosheets.[150] The embedded CNTs in the GO membranes could not only increase the interlayer distance of adjacent GO nanosheets, but also greatly improve the stability of the membranes with no obvious defects in aqueous solutions of various pH values from 1 to 12 during 180 min

of vigorous shaking. Liu *et al*. prepared the 2D graphitic carbon nitride (g-C_3N_4) nanosheets intercalated GOCN membranes through efficient assembly by GO and g-C_3N_4 nanosheets.[151] The enlarged nanochannels in the membranes were produced by the wrinkles or corrugations surrounding the g-C_3N_4 nanosheets with nanopores about 3.4 Å, thus leading to the obvious improvement in the water permeance of GOCN membranes (twice as high as that of the pure GO membranes). As the applied pressures raised from 0.1 to 0.5 MPa, the water permeance of the GOCN membranes showed an excellent linear increase, while the water permeance of the GO membranes increased nonlinearly. This phenomenon proved that the shrinkage of nanochannels in the GOCN membranes could be effectively prevented, due to the effective support for the channels by the highly rigid g-C_3N_4 nanosheets.

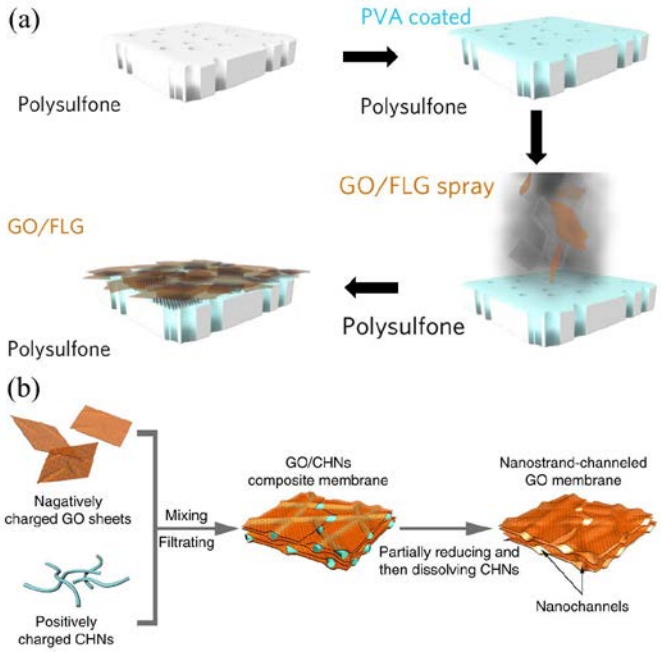

Fig. 8. (a) Fabrication of GO/FLG membranes on porous substrates by spray-coating. Reproduced with permission from ref. 54. Copyright 2017, Springer Nature. (b) Scheme of preparation process of nanostrand-channeled GO membranes. Reproduced with permission from ref. 157. Copyright 2013, Springer Nature.

Compared with organic materials, inorganic materials possess higher thermal and chemical stability, which will be beneficial for improving the stability of GO membranes. Recently, the reported inorganic materials used for intercalation into GO nanosheets mainly include SiO_2 nanoparticles,[155] TiO_2 nanoparticles,[156] copper hydroxide nanostrands,[157] halloysite nanotubes,[158] MXenes,[159] WS_2 nanosheets,[160] boron nitride nanosheets,[161] and MoS_2 nanosheets.[162] As shown in Fig. 8b, the pre-prepared positively charged copper hydroxide nanostrands (CHNs) with diameter of 2.5 nm were mixed with negatively charged GO nanosheets to prepare the GO/CHNs composite membranes by electrostatic interaction.[157] The inter-sheet spacing of GO was expanded by the presence of overlapped CHNs, as proved by the increased interlayer distance from 8.5 Å of the GO membranes to 9.9 Å of the GO/CHN membranes. To achieve higher rejection rate and improve the stability of membranes during the aqueous separation process, the GO/CHNs membranes were partially reduced in hydrazine and then dissolved the CHNs using EDTA, thus forming the nanostrand-channeled GO (NSC-GO) membranes. The well-defined nanochannels obviously improved the water permeation of the NSC-GO membranes to 10 times higher than that of the pristine GO membranes, without sacrificing the rejection performance.

As an organic-inorganic porous material, some MOFs with excellent water stability have the potential in water desalination based on size-selective diffusion.[163-165] Different from the typical 0D nanoparticles, porous MOFs will not hinder the water molecules to pass through 2D nanochannels, when they are employed as spacers to be embedded in the adjacent GO nanosheets. Guan *et al*. synthesized the uniform UiO-66 nanoporous crystals with size of around 20–30 nm by hydrothermal treatment then incorporated them into rGO nanosheet to assemble into rGO hybrid membranes by pressure-driven filtration.[166] After intercalation of the nanoporous UiO-66 crystals, both the interlayer spacings and hydrophilicities of the rGO hybrid membranes were increased, thus greatly improving the water permeation performance. Various kinds of organic, inorganic, and hybrid materials are successfully intercalate into GO sheets for enlarging the free volume of membranes and increasing the interlayer distance of GO nanochannels, thus greatly improving the transport rates of molecules. However, it is still an extraordinarily difficult task to apply physical intercalation method in preparing the GO membranes with precise sieving ability for salt ions.

3.2.2. Physical confinement

Different from the simple physical intercalation, physical confinement methods could effective restrain the out-of-plane swelling of GO laminates and manipulate the interlayer spacings, thus greatly improving the rejection of GO membranes for various salts. Abraham *et al.* employed epoxy to encapsulate the stacked GO laminates for preparation of the physically confined GO membranes (Fig. 9a). Epoxy could mechanically limit the swelling of the GO laminates on exposure to liquid water or relative high humidity environment. When the relative humidity changed from 0 to 100%, the resulting interlayer spacing of the GO laminates gradually increased from 6.4 to 9.8 Å. The GO laminates with d-spacing of 6.4 Å presented no detectable ion in the permeate side even after 5 days, while the ion permeation rates for Na^+ and K^+ appeared an exponential increase as d-spacing of the GO laminates enlarged from 7.4 to 9.8 Å.[49] Although the aligned GO laminates showed high salt rejections, yet the vertically aligned configuration limited its further application and the feasibility of scale-up production.

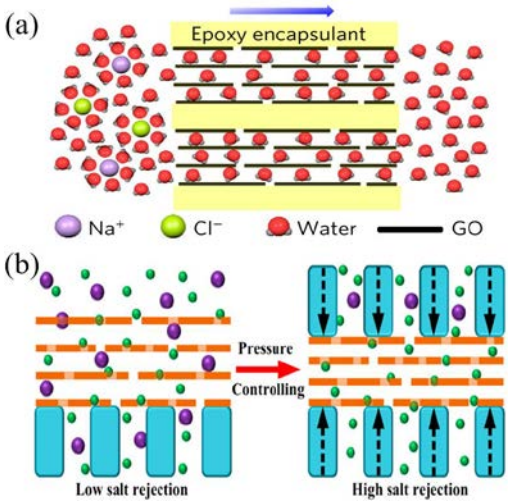

Fig. 9. (a) Schematic illustration of ion/water permeation through GO laminates encapsulated by epoxy. Reproduced with permission from ref. 49. Copyright 2017, Springer Nature. (b) Scheme of desalination by swelled and pressure controlled GO membranes. Reproduced with permission from ref. 51. Copyright 2018, American Chemical Society.

Different from isotropic materials with omnidirectional swelling behaviors, the anisotropic GO membranes with 2D configuration almost only swell on the vertical direction, thus forming larger interlayer spacing between adjacent GO nanosheets in water. Therefore, the swelling can be effectively limited by the external forces or pressures on the vertical direction, thus improving the sieving ability of GO membranes. Wei *et al*. reported that the Na_2SO_4 rejection of GO membranes could be increased from 21.3% to 85.8% after compaction at higher feed pressure, due to the narrowed transport channels.[167] Our group reported an external pressure regulation (EPR) method to restrict the swelling and interlayer spacing expansion of GO laminates in water desalination process (Fig. 9b).[51] The GO flat membranes were fixed between punched plates and porous polymer substrates in a cross-flow filtration device, which could be operated with adjustable high-resolution external pressure. At the high external pressure of 6.0 MPa, the interlayer spacing of the compressed GO membranes decreased sharply. However, this method is inconvenient to conduct in hollow fiber membrane modules, which are usually used in practical desalination process. Recently, our group further developed 3D sandwich hollow fiber membranes constructed by two exterior porous substrates and intermediate GO layers.[52] The two porous polymer substrates provide the opposite forces to limit the out-of-plane swelling and interlayer spacing expansion of GO laminates. Furthermore, the sandwich GO membranes showed robust water stability, maintaining the high rejection and permeance for over 3 days and five times of intermittent ultrasonic treatment, due to the physical confinement of GO laminates. This work provides an outstanding candidate method to manipulate the GO swelling and interlayer spacing for industrial separation applications.

3.2.3. Electric field controlling

The reported attempts to control the water permeation through GO membranes mainly concentrate on tuning the physicochemical properties and nanostructures of GO nanosheets, or the intercalation by chemical reagents, cations, and solid materials. These methods always accompanied with complicated preparation process and large energy consuming operation. Zhou *et al*. developed electrically controlled method to tune the water permeation in the interlayer spacing of GO membranes (Fig. 10a).[168] Porous thin gold layer was deposited on the top of the GO membranes supported by porous silver substrates (Fig. 10b,c), which was used as metal electrode to control the current levels across the membranes. The water permeation through the GO membranes can be precisely controlled from ultrafast permeation to complete blocking by changing the current levels, due to the current-mediated ionization of water molecules.

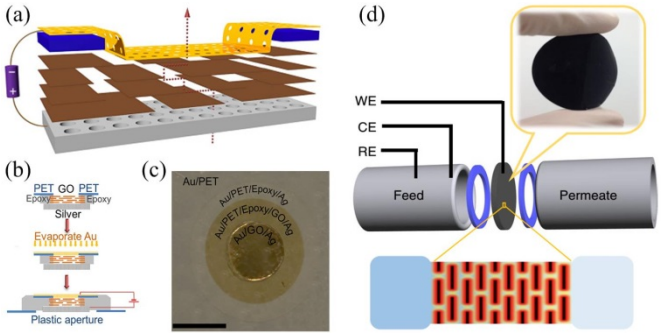

Fig. 10. (a) Schematic illustration of GO sandwich membranes applied with voltage. (b) Fabrication process of the metal–GO–metal sandwich membranes. (c) Photo of metal–GO–metal sandwich membranes. Scale bar, 6 mm. Reproduced with permission from ref. 168. Copyright 2018, Springer Nature. (d) Scheme of device for investigating the ion diffusion by nanoconfined EDLs in graphene-based nanoporous membranes. Reproduced with permission from ref. 169. Copyright 2018, Springer Nature.

Besides the water permeation, ion diffusion through layered graphene-based membranes can also be controlled by electrostatic modulation. The experimental device shown in Fig. 10d was employed to investigate the effect of interfacial electrical double layer (EDL) induced by changing the surface potential on the concentration-driven ion diffusion in the confined nanochannel of graphene-based nanoporous membranes.[169] To control the EDL enclosed between the graphene laminates, various gate potentials (V_g) were applied to the electrically conductive membranes. The produced concentration gradient drove ions to transport through the cascading nanochannels in the graphene membranes with the interlayer spacing changing from 5.4 nm to 8.0 Å. At the feed concentration of 0.1 M KCl, the normalized ion flux of the membranes with the d-spacing of 8.0 Å was three times higher than that of the membranes with the d-spacing of 5.4 nm, as the V_g increased from 0 to –0.5 V. This phenomenon had also been observed on the mesoporous carbon membranes with a pore size of 7.8 nm.[170]

3.3. Manipulating intrinsic defects/pores/edges

For GO membranes, both the interlayer nanochannels of adjacent nanosheets and intrinsic defects/pores/edges of GO nanosheets are vital for the mass transports through the membranes. In addition to control the interlayer spacing by chemical and physical methods, the manipulation of intrinsic defects/pores/edges is also very important for adjusting the mass transfer behaviors of GO membranes. There are two directions to regulate the intrinsic defects/pores/edges of GO membranes, creating nanopores for more accurate and faster separation and sealing defects/pores/edges for high selectivity and rejection.

3.3.1. Nanopore creation

Recently, porous graphene with atomic thickness has received much more attention in separation applications, owing to its unique porous structure in combination with the inherent features of graphene. Theoretical calculations show that nanoporous graphene membranes can provide a huge improvement in water flux by several orders of magnitude in contrast with conventional reverse osmosis (RO) membranes, making it one of the most promising membrane materials for water purification.[171] Surwade *et al.* created nanometre-sized pores on single-layer graphene by oxygen plasma etching method, and the prepared nanoporous graphene membranes displayed high salt rejection rate of nearly 100% in water desalination process.[172] Although the nanoporous single-layer graphene membranes show the large permeation flux and high rejection rate, the high cost and relative complex synthesis procedures make these membranes difficult to be scaled up for industrial applications. In contrast, GO with the cost-effective and easily scalable features may be a nice alternative to be applied in preparing nanoporous graphene-based membranes, which present extraordinary performance compared with pristine GO membranes. Until now, the fabrications of porous GO membranes mainly involve chemical etching, thermal reduction, combustion synthesis, and simplified Hummer's method.

Chemical etching is one of the most popular methods to produce nanopores on graphene, due to its low cost and high efficiency. As shown in Fig. 11a, nanometer-sized pores were created in GO nanosheets by chemical etching, using the mixture of ammonia solution and hydrogen peroxide.[173] The sites with oxygen-containing functional groups (less stable oxidized sp^3 domains) were preferentially to be etched, producing holes in the GO nanosheets. As the etching time was raised from 0 to 3 h, the pore sizes and the amount of pores both gradually increased (Fig. 11b, c, and d), along with the slightly decreased oxidation degree for the porous GO nanosheets. In the mechanical property test, single-layer porous GO nanosheets were weakened with the increased in-plane pores, while the etched multilayer GO films were much less sensitive to porosity. Due to the more compliant nature of the soft porous GO nanosheets, the mixed GO multilayer films containing 10 and 25 wt% etched GO nanosheets appeared a 1.7 and nearly twofold improvement in elastic modulus, respectively, in contrast with the pristine GO films. These results proved that porous GO naosheets can be used as building blocks to prepare the stable 2D separation membranes. Ying *et al.* fabricated the mesoporous GO nanosheets through a reoxidation method using $KMnO_4$, and then assembled them into porous GO membranes, which showed 2−3 times higher water flux than that of pristine GO membranes without in-plane nanopores.[174] However, the prepared porous GO membranes presented an effective sieving size of 3−5 nm, with no feasibility in salt rejection. In order to realize the high efficiency desalination, the in-plane pore sizes and interlayer spacings of porous GO membranes need to be finely controlled. Li *et al.* reported the fabrication of thermally reduced nanoporous graphene oxide (rNPGO) membranes for desalination.[48] Uniform nanopores with the average diameter of 3.14 nm were created in GO nanosheets by H_2O_2 oxidation. The presence of nanopores on GO could not only provide more transport nanochannels for water molecules but also sharply reduce the average transport distances. The prepared nanoporous rGO membranes showed a 26 times higher water flux than that of the pristine rGO membranes, proving that the introduced nanopores could greatly improve the water transport efficiency.

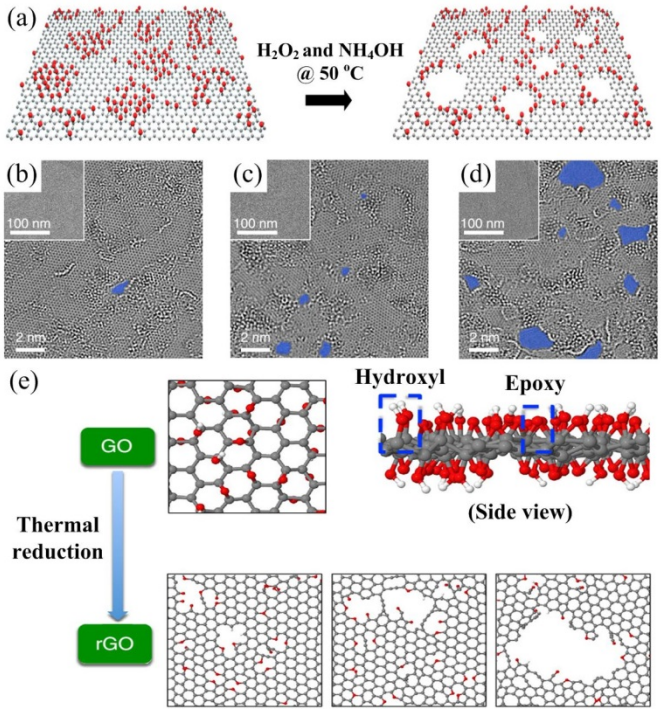

Fig. 11. (a) Scheme of preparation of porous GO nanosheets by chemical etching. TEM images of (b) pristine, (c) etched for 1 h, and (d) 3 h GO nanosheets. The blue color presented the pores in GO nanosheets. Reproduced with permission from ref. 173. Copyright 2019, Springer Nature. (e) Schematic of porous rGO formation by thermal reduction. Reproduced with permission from ref. 175. Copyright 2015, Springer Nature.

Different from the complicated chemical etching, thermal reduction method is more simple and environmentally friendly, in which the preparation of nanopores only requires heat input. In the thermal reduction process, some oxygen containing groups on GO nanosheets were removed, producing the randomly distributed nanopores in rGO nanosheets with various sizes. Lin *et al.* applied molecular dynamics (MD) simulations to precisely simulate the preparation of porous rGO nanosheets by thermal reduction (Fig. 11e), and investigated the relationship between synthesis parameters (initial GO total oxygen concentration, initial GO functional group composition, and reduction temperature) and pore sizes in rGO.[175] They found that GO materials with higher epoxy/hydroxyl ratios and total oxygen concentrations usually preferred to produce larger nanopores in the resulting rGO nanosheets. Meanwhile, the GO nanosheets with smaller total oxygen concentration and lower ratio of

epoxy/hydroxyl group would require higher reduction temperature to create nanopores with targeted size. The desalination simulation demonstrated that the porous rGO membranes prepared from the starting GO nanosheets with the oxygen concentration of 33% and the functional group ratio of 1:1 at the reduction temperature of 2000 K showed excellent performance with salt rejection of 99%.

Combustion synthesis assisted with metal salt templates is more capable to precisely control the pore sizes on the porous rGO nanosheets in contrast with the thermal reduction method. Li *et al*. reported the preparation of porous rGO nanosheets by combustion synthesis.[176] A thin layer of Zn layered double hydroxide (LDH) with defective pores was used as porous template and deposited on the surface of GO nanosheets. At the combustion process, the initial GO in the defective pores of Zn LDH was burned to create large number of nanopores in rGO. As the higher $Zn(NO_3)_2$ concentration, the defect pore size on LDH layer gradually increased, leading to the formation of larger pores on PrGO. When using 1000 g L^{-1} $Zn(NO_3)_2$ solution, the large pores with 30–45 nm size can be obtained. In the separation of Na^+ and K^+, the PrGO membranes with small pores displayed higher K^+/Na^+ selectivity (3.84), and the higher permeation ability for K^+ was attributed to the strong coordination between K^+ and carboxyl groups on PrGO.

The above described methods are usually used GO as starting materials to prepare porous GO nanosheets, in which the large amount of oxygen functional groups on GO will be reduced, thus changing the hydrophilicity and narrowing the interlayer spacing of GO. The alternative employing the oxidation of porous graphene to prepare the porous GO nanosheets may be more plausible. Lacey *et al*. synthesized the highly porous GO sheets directly from porous graphene with 2-8 nm pores by simplified Hummer's method.[177] Unlike the starting porous graphene, the prepared porous GO sheets were hydrophilic and capable to form the stable GO dispersions in water. This feature was greatly important for the preparation of porous GO membranes. Buelke *et al*. prepared porous graphene from pristine graphene sheets by controlled air oxidation, and then oxidized the porous graphene into porous GO.[59] Various porous GO membranes were fabricated on polycarbonate support by vacuum filtration to evaluate their water purification performance. The obtained porous GO membranes with short transport length showed 3.8 times higher water flux relative to pristine GO membranes. Despite that the remarkable progress has been achieved in high-density pore creation, the defects or tears with leakage pathways are inevitably formed in the preparation process of GO membranes, thus leading to a decline in rejection efficiency.

3.3.2. Defect/pore/edge sealing

In addition to punching holes, the sealing or blocking of defects/pores/edges in graphene sheets are also proved to be critical in improving the sieving ability of graphene-based membranes. O'Hern *et al*. reported the preparation of centimeter-scale nanoporous monolayer graphene with excellent sieving performance enabled by a multistep defect-sealed process.[178] When the graphene was transferred to a porous polycarbonate track etch (PCTE) support, large tears with the size about 100−200 nm were formed in the graphene/PCTE composite membrane, along with nanoscale intrinsic defects about 1−15 nm produced during the fabrication of graphene by CVD on copper. The nano-sized defects in graphene were selectively filling with hafnia by atomic layer deposition method and then the large tears were sealed using an interfacial polymerization of nylon-6,6 (Fig. 12a), leading to a centimeter-scale monolayer graphene membrane with obviously lower leakage than that of the membrane without defect sealing. After sealing treatment, nanopores were introduced in monolayer graphene by high-energy gallium ion bombardment and chemical etching of acidic potassium permanganate. The prepared nanoporous graphene membranes showed 70% rejection of $MgSO_4$ and 90% rejection of allura red under forward osmosis. Besides the sieving of salts and small molecules, the defect-sealed nanoporous monolayer graphene can also be used in dialysis.[179]

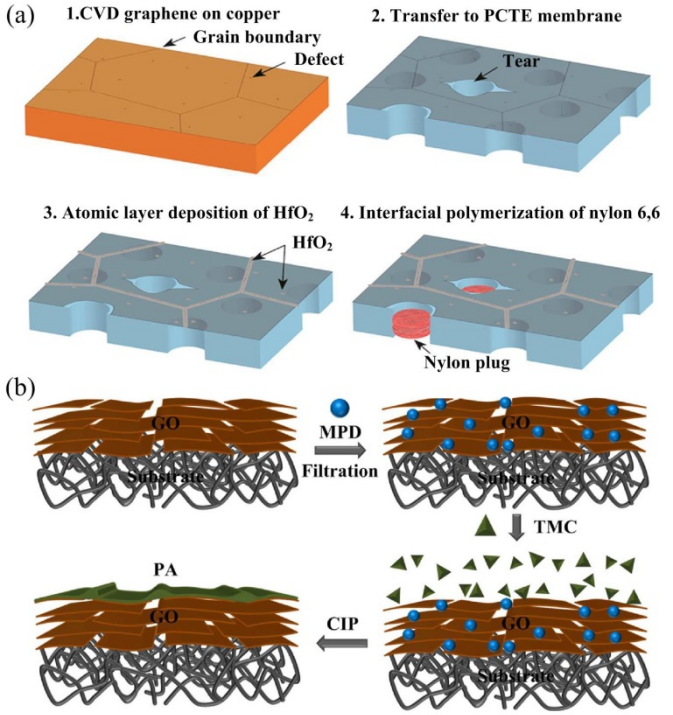

Fig. 12. (a) Schematic illustration of graphene membrane preparation and defect-sealing procedure. Reproduced with permission from ref. 178. Copyright 2015, American Chemical Society. (b) Scheme of PA-GO membrane formation by confined interfacial polymerization. Reproduced with permission from ref. 180. Copyright 2018, Elsevier.

For the multi-layered GO membranes, the sealing of intrinsic defects is also great important in realizing the high efficiency desalination. As shown in Fig. 12b, our group developed the confined interfacial polymerization strategy to prepare ultrathin PA-GO membranes with the thickness of smaller than 30 nm.[180] Due to the adsorption of negatively charged GO with oxygen functional containing groups to meta-phenylene diamine (MPD), the interfacial polymerization between MPD and trimesoyl chloride (TMC) at intrinsic defects and edges of GO sheets was conducted to produce polyamide (PA), which could refine the size of ions transport nanochannels and improve salt rejection. In the desalination test, the prepared PA-GO membranes displayed excellent NaCl rejection of 99.7%. Apart from the great future of PA-GO membranes in desalination application, the design concept of confined interfacial

polymerization may also provide a pathway to prepare other molecular separation membranes.

4. Applications of GO membranes

In the aqueous or organic solution, GO membranes will swell at vertical direction, thus the interlayer spacing will be enlarged owing to the adsorption of water molecules. The enlarged interlayer spacing in water leads to a great challenge for GO membranes to achieve the high rejection, especially for some small ions. Therefore, it is of great significance to constrain the out-of-plane swelling and precisely tune the interlayer spacing of GO membranes for achieving excellent liquid-based separation performance. In the above sections, we have discussed the various methods about accurate manipulation of transport pathways of GO membranes. This section we will discuss how to greatly improve the liquid-based separation performances of laminar GO membranes by finely controlling the transport pathways, in which the application fields can be divided as static diffusion, nanofiltration, reverse osmosis, organic solvent nanofiltration, and pervaporation.

4.1. Static diffusion

Ion sieving with specific sizes (such as Na^+, Mg^{2+}, Ca^{2+}, K^+, and Li^+) from mixed salt solutions was extremely important in sea water desalination, lithium-based batteries, and supercapacitors.[181] Considering the unique mass-transport features of GO membranes, effective solution-based ion sieving can be achieved with GO membranes under concentration-driven diffusion in static state. Joshi *et al*. prepared the laminar GO membranes by vacuum filtration and investigated the selective permeation of dissolved ions and molecules through the GO laminates under concentration-driven diffusion.[182] The GO membranes with the thickness of 5 μm displayed sharp molecular sieving performance with permeation cutoff of ∼9 Å. The small ions such as K^+ and Mg^{2+} could pass through the GO membranes, while the large ions and organic molecules displayed no detectable permeation. Furthermore, GO membranes can realize the superb ion sieving by cation-controlling method. Chen *et al*. prepared the cationic controlling GO membranes by intercalating K^+ into GO nanosheets.[50] In the ion permeation test, the Na^+, Mg^{2+}, and Ca^{2+} permeation rates of the pure GO membranes with the thickness of about 750 nm were 0.190 mol m^{-2} h^{-1}, 0.025 mol m^{-2} h^{-1}, and 0.019 mol m^{-2} h^{-1}, respectively. In contrary, the K^+ intercalated GO membranes presented no detectable permeation for Na^+, Mg^{2+}, and Ca^{2+}, proving the ion rejection rate of more than 99% compared with the pure GO membranes.

Light illumination also shows a great influence on the ion transport through GO membranes in static diffusion. Yang *et al*. used PDMS elastomer to seal layered GO membrane and then investigated its photon-electron-ion transport phenomenon.[183] When irradiated by light, cations would move thermodynamically through GO membranes at the rates much faster than the simple diffusion, because light irradiation produced the electric potential difference on GO membranes that could drive the transport of ionic species. Moreover, the flowing direction of ionic current could be controlled by changing the illumination position. When the illumination was applied to the right side of the GO membrane, the net ionic current arose from zero to about −2.27 nA within 30 s. On the contrary, if the illumination position changed to the left side, the photocurrent direction would reverse without much altering its magnitude (about +2.54 nA).

4.2. Nanofiltration and reverse osmosis

Due to its extremely thin structures and uniform 2D transport nanochannels, the laminar GO membranes display excellent nanofiltration performance. Han *et al*. prepared ultrathin (22–53 nm) graphene-based membranes by filtering reduced GO dispersion on polymer flat substrates, and then used them as nanofiltration membranes for water purification.[21] The prepared graphene membranes showed the pure water flux of 21.8 L m^{-2} h^{-1} bar^{-1} and high retention (>99%) for organic dyes based on the mechanism of physical sieving and electrostatic interaction. In addition to flat substrates, hollow fibers substrates can also be implied in preparation of GO membranes for nanofiltration. Aba *et al*. fabricated the laminar GO membranes on ceramic hollow fibers by vacuum filtration, which showed molecular weight cut off less than 300 Da in nanofiltration test.[184] Benefiting from the remarkable develop in the preparation method, GO membranes can easily realize the high efficiency rejection for small molecules. But, it is still a quite difficult task for GO membranes to precisely sieve salt ions.

To finely control ion transport through GO membranes for desalination, Zhang *et al*. prepared the surface-charged GO membranes through dip-coating a polyelectrolyte solution on the surfaces of well-stacked GO laminates.[79] Controllable charges bonded on the surfaces of GO membranes displayed dominant electrostatic repulsion forces against doubly charged co-ions (with similar charge as the membrane surface) while restraining weak electrostatic attraction to singly charged counter-ions (with opposite charge as the membrane surface). By simply changing the surface charge to positively charge or negatively charge, the ion transport was precisely tuned without sacrificing water permeation though the GO membranes. In the nanofiltration test, the positively charged GO membranes showed water permeance of 51.2 L m^{-2} h^{-1} bar^{-1} with $MgCl_2$ rejection of 93.2%, and the negatively charged GO membranes displayed water permeance of 56.8 L m^{-2} h^{-1} bar^{-1} with Na_2SO_4 rejection of 93.9%, which were far beyond the performance limitation of GO membranes.

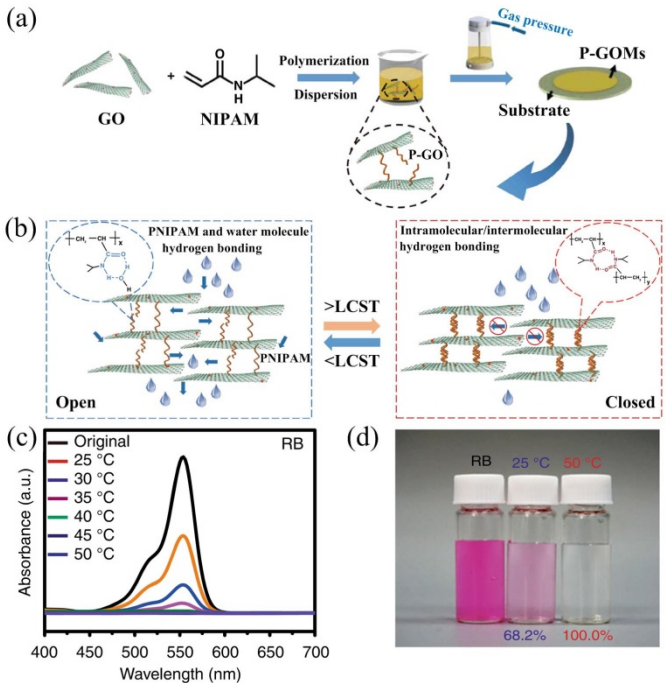

Fig. 13. (a) Preparation process of PNIPAM covalently grafted GO membranes. (b) Scheme of negative temperature-responsive behaviors in PNIPAM grafted GO membranes. (c) UV-vis absorption spectra before and after filtering rhodamine B (RB) aqueous solutions from 25 °C to 50 °C. (d) Photos of original solutions and the filtrate obtained at 25 °C and 50 °C of RB aqueous solution. Reproduced with permission from ref. 185. Copyright 2017, Springer Nature.

By covalently grafting functional polymers into GO sheets, nanofiltration performances of GO membranes can be precisely tuned by changing environmental temperature. As shown in Fig. 13a, N-isopropylacrylamide (NIPAM) monomers were covalently bonded on GO nanosheets by free-radical polymerization to form PNIPAM-grafted GO nanosheets, which were then assembled into PNIPAM grafted laminar GO membranes (P-GOMs) through pressure-driven filtration.[185] The negative temperature-responsive behaviors of P-GOMs were based on controlling the interlayer spacing by tuning the molecular configuration of PNIPAM. When the temperature was below the lower critical solution temperature (LCST) of PNIPAM-grafted GO, the PNIPAM chains presented a swollen coil structure due to the hydrogen bond force between amide group of PNIPAM and water molecules (Fig. 13b). Thus, the nanochannels for water transport between adjacent GO nanosheets would expand, showing a high water permeance. If the temperature increased higher than LCST, the PNIPAM chains would shrink because of the intramolecular hydrogen bond interaction of PNIPAM, leading to a smaller lamellar distance of P-GOMs and lower water permeance. In the permeation test, the P-GOMs with the thickness of 1.1 μm showed an average water flux of 12.4 L m^{-2} h^{-1} bar^{-1} at 25 °C, and decreased to 1.8 L m^{-2} h^{-1} bar^{-1} as the temperature increased up to 50 °C. The nanofiltration performance of P-GOMs was also influenced by the temperature, with the high rejection rate (100%) for RB at 50 °C (Fig. 13c and d). Furthermore, positive temperature-responsive P-GOMs can also be obtained by decreasing the PNIPAM grafting density, and the membranes would display larger water permeances when the temperature was higher than LCST.[186] This result was caused by the shrinking of sparse PNIPAM chain when temperature exceeded LCST, expanding more space in nanochannels for water transport.

A CO_2-responsive GO-based nanofiltration membrane can also be prepared by intercalating the positively charged polymer. Dong *et al*. synthesized the CO_2-responsive GO-based nanofiltration membranes by electrostatic forces and π–π interactions driven complexation reaction between poly(N,N-diethylaminoethyl methacrylate) with a pyrene ending group (Py-PDEAEMA) and GO.[187] When passing CO_2 through the solution, the tertiary amine groups in Py-PDEAEMA were protonated, which make the polymer soluble in water, thus narrowing the water flow channel and leading to the low water permeation. The decreased water permeability can be almost fully recovered when Ar was bubbled into the solution. In the four cycles of dye rejection test, CO_2 and Ar were alternately introduced into the solution. Although the water permeability of the Py-PDEAEMA/GO membranes swung from 13.6 L m^{-2} h^{-1} bar^{-1} to 48.5 L m^{-2} h^{-1} bar^{-1} upon CO_2 and Ar bubbling, the dye rejection rates were always at high level of 98.9% and 96.5% for RB and MO, respectively.

The swelling of GO membranes causes the poor rejection for monovalent salt Na^+ and K^+. To achieve the high efficiency desalination, our group employed an EPR system to precisely control the out-of-plane expansion of GO membranes.[51] In cross-flow filtration test, the compressed GO membranes displayed the outstanding desalination performances with KCl, NaCl, and $CaCl_2$ rejections of 94%, 97%, and 98%, respectively, due to the narrowed interlayer spacing by external pressure. The accompanied water permeance was as high as 25 L m^{-2} h^{-1} under the feed pressure of 2 bar, which was larger than that of the most polymer membranes possessing similar salt rejection. To open up the possibility of practical application, the ultrastable 3D sandwich hollow fiber membranes were further developed.[52] Benefiting from the confined interlayer spacing of 8.6 Å, the robust sandwich GO membranes showed high permeances and impressive desalination performances with NaCl, $MgCl_2$, $MgSO_4$ and Na_2SO_4 rejections of 97.5%, 98.0%, 98.5%, and 99.1%, respectively, which were obviously larger than those of traditional GO membranes, usually lower than 40%.

4.3. Organic solvent nanofiltration

As a widely-applied technology in the chemical and pharmaceutical industries, organic solvent nanofiltration (OSN) membranes receive tremendous attention. Compared with the commonly used polymeric or ceramic OSN membranes, GO membranes possess ultrathin separating layers and controllable 2D transport nanochannels, providing them with great potential in organic solvent sieving. Huang *et al*. prepared the GO membranes with nylon substrates by vacuum filtration to investigate its semipermeability in organic solvents.[188] The prepared GO membranes showed excellent size sieving performance for different solutes in ethanol. The permeation rates gradually increased when the sizes of solute molecules

decreased. Due to the smallest molecular size among the tested molecules, acetone displayed the largest permeation rate of 1.43 ± 0.07 mol m^{-2} h^{-1}, which was about 25 times higher than that of pyrene. In contrast, the large molecules such as lumogen red 300 could not pass through the GO membranes with no detected molecule permeation even after 1 week. The semipermeability of the GO membranes could be finely controlled by thermal annealing treatment. When the annealing temperature increased from 100 to 140 °C, the permeation rates of p-xylene in ethanol decreased from 0.34 ± 0.01 mol m^{-2} h^{-1} to 0.040 ± 0.005 mol m^{-2} h^{-1}, because of the narrowed nanochannels and reduced oxygen-containing groups in GO after thermal annealing treatment. To further improve the organic solvent permeation rate, Yang *et al*. fabricated the highly laminated GO (HLGO) membranes by vacuum filtration.[58] Benefiting from the GO flakes with large lateral size (10–20 μm) and relatively narrow size distribution, the prepared GO membranes showed superior laminar structure with smooth 2D capillaries in contrast with the membranes prepared from smaller flakes (0.1–0.6 μm). This result could be attributed to stronger interlayer interactions between larger overlapping areas, which were beneficial for eliminating the occasional wrinkles and corrugation, thus resulting in the formation of smoother 2D capillaries in GO membranes with large lateral sizes of GO flakes.[189] In the nanofiltration experiments with methanol solutions, the prepared HLGO membranes with the thickness of 8 nm showed fast solvent permeation and 100% rejection for all the dye molecules such as chrysoidine G, brilliant blue, and rose bengal. The excellent organic solvent permeation and sieving performances could be attributed to the randomly distributed pinholes interconnected by short GO nanochannels with a width of 10 Å. For the GO membranes with small GO flakes, more defects/pores/edges and much shortened interlayer nanochannels may cause the increase of permeation.[58,189]

Different from the GO, the chemical reduced rGO nanosheets possesses strong hydrophobicity and narrowed interlayer spacing, which was beneficial for rGO membranes to obtain the high solvent permeation and precise molecular sieving. Huang *et al*. prepared rGO dispersion from the reduction of GO by hydrazine in an alkaline aqueous solution, which was then assembled on nylon and anodic aluminum oxide supports to obtain the solvent solvated rGO (S-rGO) membranes.[190] The prepared S-rGO membranes displayed outstanding stability in organic solvents, even to strong acidic, alkaline. For organic solvent nanofiltration, the negatively charged S-rGO membranes with the thickness of 18 nm presented complete rejection for negatively charged evans blue molecules in methanol with an ultrafast permeance of 75.3 L m^{-2} h^{-1} bar^{-1}, due to its solvent solvated microstructures.

4.4. Pervaporation

The intrinsic hydrophilicity of GO nanosheets and the ultrafast selective water permeation through graphene nanochannels endow GO-based membranes with great promise in purifying aqueous organic solutions by the pervaporation technology. Huang *et al*. prepared the GO membranes on ceramic hollow fibers by vacuum-assisted suction for separation of aqueous organic solution.[56] In the pervaporation separation of dimethyl carbonate/water mixtures, the GO membranes showed high permeation flux of 1702 g m^{-2} h^{-1} with the permeate water content at 95.2 wt%. Moreover, to improve the pervaporation performance, functional polymers are introduced into GO membranes. Ang *et al*. employed the zwitterionic copolymers, poly(glycidyl methacrylate-sulfobetaine methacrylate) [poly(GMA-SBMA)] to be embedded into GO for preparation of GO–poly(GMA-SBMA) framework.[191] After the pressure-assisted filtration, GO–poly(GMA-SBMA) was assembled on the PSf supports to form the GO membranes incorporated with zwitterionic copolymers (Z-GOM). Due to the incorporation of hydrophilic poly(GMA-SBMA), the hydrophilicities of membranes were greatly improved as the water contact angles decreased from 64° to 30°. When increased the adding amounts of poly(GMA-SBMA), the interlayer distance between adjacent GO nanosheets expanded, enhancing the water permeation through the GO membranes. In the pervaporation purification of 70 wt% aqueous isopropanol solution, the GO membranes incorporated with poly(GMA-SBMA) showed the permeation flux of 1102 g m^{-2} h^{-1} and permeate water content of 99.6 wt%.

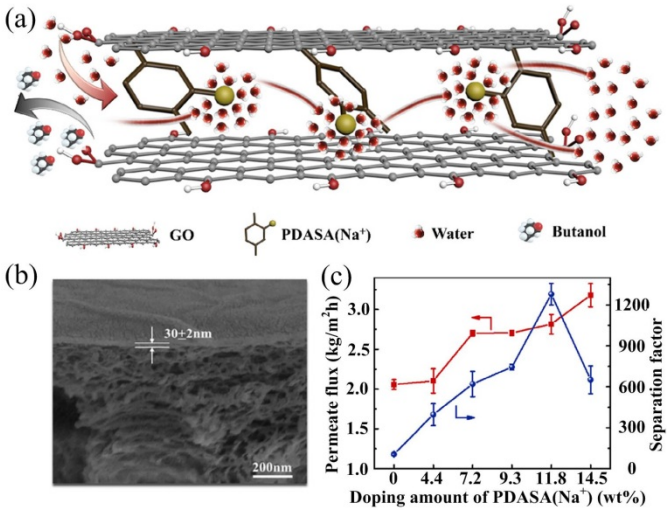

Fig. 14 (a) Schematic diagram of molecular transport in PDASA(Na^+)/GO membranes. (b) Cross-sectional SEM image of PDASA(Na^+)/GO membranes. (c) Influence of doping amount of PDASA(Na^+) in membranes on the flux and water/butanol separation factor at 313 K. Reproduced with permission from ref. 192. Copyright 2020, John Wiley and Sons.

The functional small molecules can be covalently bonded on the GO nanosheets to facilitate the molecular transport through graphene-based membranes in pervaporation process. As shown in Fig. 14a, the multifunctional sodium 1,4-phenylenediamine-2-sulfonate (PDASA(Na^+)) was intercalated into GO nanosheets as high-efficiency water transport promoter.[192] The amine groups on PDASA(Na^+) covalently bonded with GO by nucleophilic addition reaction to control the assembly of GO nanosheets and produce the strong cross-linking interlayer structures, thus limiting the swelling of GO membranes in water. As a high-efficiency water transport promoter, the ionized sulfonate groups on PDASA(Na^+) showed a critical role in accelerating the water sorption by providing

electrostatic interaction sites and improving the water-selective diffusion by endowing higher water mobility. As the adding amounts of PDASA(Na^+) gradually increased, the PDASA(Na^+)/GO membranes showed the higher permeation flux and water/butanol separation factor. When the adding amount was 11.8 wt%, the PDASA(Na^+)/GO membranes with thicknesses about 30 nm achieved the excellent pervaporation performance with the permeation flux of 2880 g m^{-2} h^{-1} and water/butanol separation factor of 1366 (Fig. 14b and c), which were 38.5% and 11 times larger than that of pure GO membranes, respectively, owing to the existence of robust cross-linking GO nanochannels and sulfonate water promoters.

5. Conclusions and outlook

In summary, the rapid development in design and preparation of GO membranes, especially the remarkable progresses in controlling the transport pathways have been achieved. Benefitting from the extremely thin structures, tunable physicochemical properties, and controllable transport nanochannels, the prepared laminar GO membranes display unparalleled sieving performances for small molecules/ions in static diffusion, pressure-driven filtration, and pervaporation. With deep insights into transport mechanisms, the delicate manipulations of transport pathways including interlayer nanochannels formed by adjacent nanosheet interactions and intrinsic defects/pores/edges of GO nanosheets are successfully achieved by various chemical and physical methods. Although GO membranes show ultrafast and highly selective sieving capability in liquid separations, there are still several challenges for GO membranes in the future development, including the improvement of membrane stability, optimization in membrane fabrication technology, and practical application in industrial field. To overcome these challenges, we need to make efforts in the following aspects. 1) Optimization of GO nanosheets. More effective and low-cost physical or chemical approaches are required to produce GO nanosheets with precise controlling in their physiochemical properties such as lateral sizes, functional groups, and pores, which will be beneficial for improving the microstructures and performances of GO membranes. 2) Delicate manipulation of transport pathways. The transport pathways in GO membranes including interlayer nanochannels between adjacent GO nanosheets and intrinsic defects/pores/edges of GO nanosheets have great influence on the separation performances of GO membranes. More simple and accurate methods including molecular intercalation, physical fixation, and pore functionalization need to be developed for controlling the transport channels of GO membranes at angstrom level. 3) Developing novel GO membranes. To realize the application in industrial fields, novel GO membranes with long term stability and strong mechanical strength should be developed to resist the high pressures in practical liquid separation applications. Several promising strategies such as chemical crosslinking and physical confinement may be the outstanding candidates to accomplish this purpose. In general, we hope that the discussion and analysis of the strategies and mechanisms for controlling transport pathways will be conducive to the development of GO membranes in separation applications.

Conflicts of interest

There are no conflicts to declare.

Acknowledgements

This work was supported by the National Natural Science Foundation of China (Grant No. 51708252) and the Fundamental Research Funds for the Central Universities (Grant No. 21617322)

Notes and references

1. B. Mi, *Science*, 2014, **343**, 740-742.
2. G. Liu, W. Jin and N. Xu, *Chem. Soc. Rev.*, 2015, **44**, 5016-5030.
3. W. Li, P. Su, Z. Li, Z. Xu, F. Wang, H. Ou, J. Zhang, G. Zhang and E. Zeng, *Nat. Commun.*, 2017, **8**, 406.
4. W. Li, W. Wu, Z. Li, J. Shi and Y. Xia, *J. Mater. Chem. A*, 2018, **6**, 16333-16340.
5. P. Su, X. Zhang, Y. Li, H. Chen, Q. Meng and G. Zhang, *AIChE J.*, 2019, **65**, e16693.
6. S. Kim, H. Wang and Y. M. Lee, *Angew. Chem. Int. Ed.*, 2019, **58**, 17512-17527.
7. L. M. Robeson, *J. Membr. Sci.*, 2008, **320**, 390-400.
8. H. B. Park, J. Kamcev, L. M. Robeson, M. Elimelech and B. D. Freeman, *Science*, 2017, **356**, eaab0530.
9. Z. Yang, H. Guo, Z. Yao, Y. Mei and C. Y. Tang, *Environ. Sci. Technol.*, 2019, **53**, 5301-5308.
10. M. Y. Jeon, D. Kim, P. Kumar, P. S. Lee, N. Rangnekar, P. Bai, M. Shete, B. Elyassi, H. S. Lee, K. Narasimharao, S. N. Basahel, S. Al-Thabaiti, W. Xu, H. J. Cho, E. O. Fetisov, R. Thyagarajan, R. F. DeJaco, W. Fan, K. A. Mkhoyan, J. I. Siepmann and M. Tsapatsis, *Nature*, 2017, **543**, 690-694.
11. D. Kim, M. Y. Jeon, B. L. Stottrup and M. Tsapatsis, *Angew. Chem. Int. Ed.*, 2018, **57**, 480-485.
12. B. Min, S. Yang, A. Korde, Y. H. Kwon, C. W. Jones and S. Nair, *Angew. Chem. Int. Ed.*, 2019, **58**, 8201-8205.
13. Y. Peng, Y. Li, Y. Ban, H. Jin, W. Jiao, X. Liu and W. Yang, *Science*, 2014, **346**, 1356-1359.
14. T. Rodenas, I. Luz, G. Prieto, B. Seoane, H. Miro, A. Corma, F. Kapteijn, F. X. Llabrés i Xamena and J. Gascon, *Nat. Mater.*, 2015, **14**, 48-55.
15. X. Wang, C. Chi, K. Zhang, Y. Qian, K. M. Gupta, Z. Kang, J. Jiang and D. Zhao, *Nat. Commun.*, 2017, **8**, 14460.
16. W. Li, *Prog. Mater. Sci.*, 2019, **100**, 21-63.
17. W. Zhang, L. Zhang, H. Zhao, B. Li and H. Ma, *J. Mater. Chem. A*, 2018, **6**, 13331-13339.
18. H. Yang, L. Yang, H. Wang, Z. Xu, Y. Zhao, Y. Luo, N. Nasir, Y. Song, H. Wu, F. Pan and Z. Jiang, *Nat. Commun.*, 2019, **10**, 2101.
19. Y. Kang, Y. Xia, H. Wang and X. Zhang, *Adv. Funct. Mater.*, 2019, **29**, 1902014.
20. R. R. Nair, H. A. Wu, P. N. Jayaram, I. V. Grigorieva and A. K. Geim, *Science*, 2012, **335**, 442-444.
21. Y. Han, Z. Xu and C. Gao, *Adv. Funct. Mater.*, 2013, **23**, 3693-3700.
22. W. Ying, K. Zhou, Q. Hou, D. Chen, Y. Guo, J. Zhang, Y. Yan, Z. Xu and X. Peng, *J. Mater. Chem. A*, 2019, **7**, 15062-15067.
23. L. Ding, Y. Wei, Y. Wang, H. Chen, J. Caro and H. Wang, *Angew. Chem. Int. Ed.*, 2017, **56**, 1825-1829.

24. L. Ding, Y. Wei, L. Li, T. Zhang, H. Wang, J. Xue, L. Ding, S. Wang, J. Caro and Y. Gogotsi, *Nat. Commun.*, 2018, **9**, 155.
25. G. Liu, J. Shen, Y. Ji, Q. Liu, G. Liu, J. Yang and W. Jin, *J. Mater. Chem. A*, 2019, **7**, 12095-12104.
26. Z. Wang, Q. Tu, S. Zheng, J. J. Urban, S. Li and B. Mi, *Nano Lett.*, 2017, **17**, 7289-7298.
27. L. Ries, E. Petit, T. Michel, C. C. Diogo, C. Gervais, C. Salameh, M. Bechelany, S. Balme, P. Miele, N. Onofrio and D. Voiry, *Nat. Mater.*, 2019, **18**, 1112-1117.
28. H. Li, T. Ko, M. Lee, H. Chung, S. S. Han, K. H. Oh, A. Sadmani, H. Kang and Y. Jung, *Nano Lett.*, 2019, **19**, 5194-5204.
29. Y. Wang, N. Wu, Y. Wang, H. Ma, J. Zhang, L. Xu, M. K. Albolkany and B. Liu, *Nat. Commun.*, 2019, **10**, 2500.
30. L. F. Villalobos, M. T. Vahdat, M. Dakhchoune, Z. Nadizadeh, M. Mensi, E. Oveisi, D. Campi, N. Marzari and K. V. Agrawal, *Sci. Adv.*, 2020, **6**, eaay9851.
31. B. Sun, Y. Kim, Y. Wang, H. Wang, J. Kim, X. Liu and M. Lee, *Nat. Mater.*, 2018, **17**, 599-604.
32. C. Chen, J. Wang, D. Liu, C. Yang, Y. Liu, R. S. Ruoff and W. Lei, *Nat. Commun.*, 2018, **9**, 1902.
33. S. Zhang, J. Zhang, W. Fang, Y. Zhang, Q. Wang and J. Jin, *Nano Lett.*, 2018, **18**, 6563-6569.
34. W. Li, Y. Zhang, Q. Li and G. Zhang, *Chem. Eng. Sci.*, 2015, **135**, 232-257.
35. K. Huang, G. Liu, J. Shen, Z. Chu, H. Zhou, X. Gu, W. Jin and N. Xu, *Adv. Funct. Mater.*, 2015, **25**, 5809-5815.
36. G. Liu, J. Shen, Q. Liu, G. Liu, J. Xiong, J. Yang and W. Jin, *J. Membr. Sci.*, 2018, **548**, 548-558.
37. C. Lee, X. Wei, J. W. Kysar and J. Hone, *Science*, 2008, **321**, 385-388.
38. W. Li, Y. Zhang, Z. Xu, A. Yang, Q. Meng and G. Zhang, *Chem. Commun.*, 2014, **50**, 15867-15869.
39. P. Sun, K. Wang and H. Zhu, *Adv. Mater.*, 2016, **28**, 2287-2310.
40. J. Zhao, G. He, S. Huang, L. F. Villalobos, M. Dakhchoune, H. Bassas and K. V. Agrawal, *Sci. Adv.*, 2019, **5**, eaav1851.
41. J. S. Bunch, S. S. Verbridge, J. S. Alden, A. M. van der Zande, J. M. Parpia, H. G. Craighead and P. L. McEuen, *Nano Lett.*, 2008, **8**, 2458-2462.
42. V. Berry, *Carbon*, 2013, **62**, 1-10.
43. Y. Yang, X. Yang, L. Liang, Y. Gao, H. Cheng, X. Li, M. Zou, R. Ma, Q. Yuan and X. Duan, *Science*, 2019, **364**, 1057.
44. S. Pei, Q. Wei, K. Huang, H. Cheng and W. Ren, *Nat. Commun.*, 2018, **9**, 145.
45. Y. Wei, Y. Zhang, X. Gao, Z. Ma, X. Wang and C. Gao, *Carbon*, 2018, **139**, 964-981.
46. D. C. Marcano, D. V. Kosynkin, J. M. Berlin, A. Sinitskii, Z. Sun, A. Slesarev, L. B. Alemany, W. Lu and J. M. Tour, *ACS Nano*, 2010, **4**, 4806-4814.
47. S. Zheng, Q. Tu, J. J. Urban, S. Li and B. Mi, *ACS Nano*, 2017, **11**, 6440-6450.
48. Y. Li, W. Zhao, M. Weyland, S. Yuan, Y. Xia, H. Liu, M. Jian, J. Yang, C. D. Easton, C. Selomulya and X. Zhang, *Environ. Sci. Technol.*, 2019, **53**, 8314-8323.
49. J. Abraham, K. S. Vasu, C. D. Williams, K. Gopinadhan, Y. Su, C. T. Cherian, J. Dix, E. Prestat, S. J. Haigh, I. V. Grigorieva, P. Carbone, A. K. Geim and R. R. Nair, *Nat. Nanotechnol.*, 2017, **12**, 546-550.
50. L. Chen, G. Shi, J. Shen, B. Peng, B. Zhang, Y. Wang, F. Bian, J. Wang, D. Li, Z. Qian, G. Xu, G. Liu, J. Zeng, L. Zhang, Y. Yang, G. Zhou, M. Wu, W. Jin, J. Li and H. Fang, *Nature*, 2017, **550**, 380-383.
51. W. Li, W. Wu and Z. Li, *ACS Nano*, 2018, **12**, 9309-9317.
52. W. Wu, J. Su, M. Jia, W. Zhong, Z. Li and W. Li, *J. Mater. Chem. A*, 2019, **7**, 13007-13011.
53. M. Sun and J. Li, *Nano Today*, 2018, **20**, 121-137.
54. A. Morelos-Gomez, R. Cruz-Silva, H. Muramatsu, J. Ortiz-Medina, T. Araki, T. Fukuyo, S. Tejima, K. Takeuchi, T. Hayashi, M. Terrones and M. Endo, *Nat. Nanotechnol.*, 2017, **12**, 1083-1088.
55. H. Huang, Y. Ying and X. Peng, *J. Mater. Chem. A*, 2014, **2**, 13772–13782.
56. K. Huang, G. Liu, Y. Lou, Z. Dong, J. Shen and W. Jin, *Angew. Chem. Int. Ed.*, 2014, **53**, 6929-6932.
57. Q. Wang, G. Zhao, C. Li and H. Meng, *J. Membr. Sci.*, 2019, **586**, 177-184.
58. Q. Yang, Y. Su, C. Chi, C. T. Cherian, K. Huang, V. G. Kravets, F. C. Wang, J. C. Zhang, A. Pratt, A. N. Grigorenko, F. Guinea, A. K. Geim and R. R. Nair, *Nat. Mater.*, 2017, **16**, 1198.
59. C. Buelke, A. Alshami, J. Casler, Y. Lin, M. Hickner and I. H. Aljundi, *J. Membr. Sci.*, 2019, **588**, 117-195.
60. W. L. Xu, C. Fang, F. Zhou, Z. Song, Q. Liu, R. Qiao and M. Yu, *Nano Lett.*, 2017, **17**, 2928-2933.
61. C. Tsou, Q. An, S. Lo, M. De Guzman, W. Hung, C. Hu, K. Lee and J. Lai, *J. Membr. Sci.*, 2015, **477**, 93-100.
62. C. Chi, X. Wang, Y. Peng, Y. Qian, Z. Hu, J. Dong and D. Zhao, *Chem. Mater.*, 2016, **28**, 2921-2927.
63. M. Fathizadeh, H. N. Tien, K. Khivantsev, J. T. Chen and M. Yu, *J. Mater. Chem. A*, 2017, **5**, 20860-20866.
64. J. Wang, Z. Yuan, X. Wu, Y. Li, J. Chen and Z. Jiang, *Adv. Funct. Mater.*, 2019, **29**, 1900819.
65. A. Akbari, P. Sheath, S. T. Martin, D. B. Shinde, M. Shaibani, P. C. Banerjee, R. Tkacz, D. Bhattacharyya and M. Majumder, *Nat. Commun.*, 2016, **7**, 10891.
66. J. Zhong, W. Sun, Q. Wei, X. Qian, H. M. Cheng and W. Ren, *Nat. Commun.*, 2018, **9**, 3484.
67. H. W. Kim, H. W. Yoon, S. Yoon, B. M. Yoo, B. K. Ahn, Y. H. Cho, H. J. Shin, H. Yang, U. Paik, S. Kwon, J. Choi and H. B. Park, *Science*, 2013, **342**, 91-95.
68. H. M. Hegab and L. Zou, *J. Membr. Sci.*, 2015, **484**, 95-106.
69. J. Zhao, Y. Zhu, F. Pan, G. He, C. Fang, K. Cao, R. Xing and Z. Jiang, *J. Membr. Sci.*, 2015, **487**, 162-172.
70. X. Song, R. S. Zambare, S. Qi, B. N. I. L. Sowrirajalu, A. P. James Selvaraj, C. Y. Tang and C. Gao, *ACS Appl. Mater. Interfaces*, 2017, **9**, 41482-41495.
71. J. Borges and J. F. Mano, *Chem. Rev.*, 2014, **114**, 8883-8942.
72. E. Ahn, H. Gaiji, T. Kim, M. Abderrabba, H. Lee and B. Kim, *J. Membr. Sci.*, 2019, **585**, 191-198.
73. M. Diba, D. W. H. Fam, A. R. Boccaccini and M. S. P. Shaffer, *Prog. Mater. Sci.*, 2016, **82**, 83-117.
74. S. J. An, Y. Zhu, S. H. Lee, M. D. Stoller, T. Emilsson, S. Park, A. Velamakanni, J. An and R. S. Ruoff, *J. Phys. Chem. Lett.*, 2010, **1**, 1259-1263.
75. S. A. Hasan, J. L. Rigueur, R. R. Harl, A. J. Krejci, I. Gonzalo-Juan, B. R. Rogers and J. H. Dickerson, *ACS Nano*, 2010, **4**, 7367-7372.
76. M. Wang, L. D. Duong, J. Oh, N. T. Mai, S. Kim, S. Hong, T. Hwang, Y. Lee and J. Nam, *ACS Appl. Mater. Interfaces*, 2014, **6**, 1747-1753.
77. J. Deng, Y. You, H. Bustamante, V. Sahajwalla and R. K. Joshi, *Chem. Sci.*, 2017, **8**, 1701-1704.
78. P. Sun, F. Zheng, M. Zhu, Z. Song, K. Wang, M. Zhong, D. Wu, R. B. Little, Z. Xu and H. Zhu, *ACS Nano*, 2014, **8**, 850-859.
79. M. Zhang, K. Guan, Y. Ji, G. Liu, W. Jin and N. Xu, *Nat. Commun.*, 2019, **10**, 1253.
80. T. Yang, H. Lin, X. Zheng, K. P. Loh and B. Jia, *J. Mater. Chem. A*, 2017, **5**, 16537-16558.
81. C. Yeh, K. Raidongia, J. Shao, Q. Yang and J. Huang, *Nat. Chem.*, 2015, **7**, 166-170.

82. P. Zhang, J. Gong, G. Zeng, B. Song, S. Fang, M. Zhang, H. Liu, S. Huan, P. Peng, Q. Niu, D. Wang and J. Ye, *Sep. Purif. Technol.*, 2019, **220**, 309-319.
83. L. Qiu, X. Zhang, W. Yang, Y. Wang, G. P. Simon and D. Li, *Chem. Commun.*, 2011, **47**, 5810-5812.
84. H. Huang, R. K. Joshi, K. K. H. De Silva, R. Badam and M. Yoshimura, *J. Membr. Sci.*, 2019, **572**, 12-19.
85. Z. Li, Y. Xing, X. Fan, L. Lin, A. Meng and Q. Li, *Desalination*, 2018, **443**, 130-136.
86. B. Qi, X. He, G. Zeng, Y. Pan, G. Li, G. Liu, Y. Zhang, W. Chen and Y. Sun, *Nat. Commun.*, 2017, **8**, 825.
87. H. Liu, H. Wang and X. Zhang, *Adv. Mater.*, 2015, **27**, 249-254.
88. E. Yang, M. Ham, H. B. Park, C. Kim, J. Song and I. S. Kim, *J. Membr. Sci.*, 2018, **547**, 73-79.
89. J. Kim, S. E. Lee, S. Seo, J. Y. Woo and C. S. Han, *J. Membr. Sci.*, 2019, **592**, 117394.
90. K. H. Thebo, X. Qian, Q. Zhang, L. Chen, H. Cheng and W. Ren, *Nat. Commun.*, 2018, **9**, 1486.
91. W. Hung, C. Tsou, M. De Guzman, Q. An, Y. Liu, Y. Zhang, C. Hu, K. Lee and J. Lai, *Chem. Mater.*, 2014, **26**, 2983-2990.
92. H. Lin, S. Dangwal, R. Liu, S. Kim, Y. Li and J. Zhu, *J. Membr. Sci.*, 2018, **563**, 336-344.
93. N. Meng, W. Zhao, E. Shamsaei, G. Wang, X. Zeng, X. Lin, T. Xu, H. Wang and X. Zhang, *J. Membr. Sci.*, 2018, **548**, 363-371.
94. M. Liu, J. Guo, S. Japip, T. Jia, D. Shao, S. Zhang, W. Li, J. Wang, X. Cao and S. Sun, *J. Mater. Chem. A*, 2019, **7**, 3170-3178.
95. Y. Qian, X. Zhang, C. Liu, C. Zhou and A. Huang, *Desalination*, 2019, **460**, 56-63.
96. B. Feng, K. Xu and A. Huang, *Desalination*, 2016, **394**, 123-130.
97. P. Zhang, J. Gong, G. Zeng, C. Deng, H. Yang, H. Liu and S. Huan, *Chem. Eng. J.*, 2017, **322**, 657-666.
98. Z. Jia and Y. Wang, *J. Mater. Chem. A*, 2015, **3**, 4405-4412.
99. G. Yang, Z. Xie, M. Cran, D. Ng, C. D. Easton, M. Ding, H. Xu and S. Gray, *J. Mater. Chem. A*, 2019, **7**, 19682-19690.
100. Y. Zhang, K. Su and Z. Li, *J. Membr. Sci.*, 2018, **563**, 718-725.
101. X. Tang, Y. Qu, S. Deng, Y. Tan, Q. Zhang and Q. Liu, *J. Mater. Chem. A*, 2018, **6**, 22590-22598.
102. J. Yang, D. Gong, G. Li, G. Zeng, Q. Wang, Y. Zhang, G. Liu, P. Wu, E. Vovk, Z. Peng, X. Zhou, Y. Yang, Z. Liu and Y. Sun, *Adv. Mater.*, 2018, **30**, 1705775.
103. J. Ran, C. Chu, T. Pan, L. Ding, P. Cui, C. Fu, C. Zhang and T. Xu, *J. Mater. Chem. A*, 2019, **7**, 8085-8091.
104. Y. T. Nam, J. Choi, K. M. Kang, D. W. Kim and H. T. Jung, *ACS Appl. Mater. Interfaces*, 2016, **8**, 27376-27382.
105. M. Lim, Y. Choi, J. Kim, K. Kim, H. Shin, J. Kim, D. M. Shin and J. Lee, *J. Membr. Sci.*, 2017, **521**, 1-9.
106. C. Kim, S. An, J. Lee, Q. Zeng and J. D. Fortner, *ACS Appl. Mater. Interfaces*, 2019, **11**, 924-929.
107. P. S. Parsamehr, M. Zahed, M. A. Tofighy, T. Mohammadi and M. Rezakazemi, *Desalination*, 2019, **468**, 114079.
108. T. Gao, H. Wu, L. Tao, L. Qu and C. Li, *J. Mater. Chem. A*, 2018, **6**, 19563-19569.
109. Y. Song, R. Li, F. Pan, Z. He, H. Yang, Y. Li, L. Yang, M. Wang, H. Wang and Z. Jiang, *J. Mater. Chem. A*, 2019, **7**, 18642-18652.
110. S. Wang, Y. Xie, G. He, Q. Xin, J. Zhang, L. Yang, Y. Li, H. Wu, Y. Zhang, M. D. Guiver and Z. Jiang, *Angew. Chem. Int. Ed.*, 2017, **56**, 14246-14251.
111. A. Suri, L. Calzavarini, A. B. Strunck, G. Magnacca and V. Boffa, *Ind. Eng. Chem. Res.*, 2019, **58**, 18788-18797.
112. D. Zhao, J. Zhao, Y. Ji, G. Liu, S. Liu and W. Jin, *J. Membr. Sci.*, 2018, **567**, 311-320.
113. J. J. Lu, Y. H. Gu, Y. Chen, X. Yan, Y. J. Guo and W. Z. Lang, *Sep. Purif. Technol.*, 2019, **210**, 737-745.
114. X. L. Xu, F. W. Lin, Y. Du, X. Zhang, J. Wu and Z. K. Xu, *ACS Appl. Mater. Interfaces*, 2016, **8**, 12588-12593.
115. J. Hu, Z. Liu, K. Deng, Z. Chen, Q. Cai, Y. Faraj, R. Xie, X. Ju, W. Wang and L. Chu, *J. Membr. Sci.*, 2019, **591**, 117345.
116. H. Shen, N. Wang, K. Ma, L. Wang, G. Chen and S. Ji, *J. Membr. Sci.*, 2017, **527**, 43-50.
117. W. W. Lei, H. Li, L. Y. Shi, Y. F. Diao, Y. L. Zhang, R. Ran and W. Ni, *Appl. Surf. Sci.*, 2017, **404**, 230-237.
118. W. Zhang, J. Jia, Y. Qiu and K. Pan, *Adv. Mater. Interfaces*, 2018, **5**, 1701386.
119. Z. Chen, Z. Liu, J. Hu, Q. Cai, X. Li, W. Wang, Y. Faraj, X. Ju, R. Xie and L. Chu, *J. Membr. Sci.*, 2020, **595**, 117510.
120. J. Song, H. Yu, M. Ham and I. S. Kim, *Nano Lett.*, 2018, **18**, 5506-5513.
121. S. Kim, J. Nham, Y. S. Jeong, C. S. Lee, S. H. Ha, H. B. Park and Y. J. Lee, *Chem. Mater.*, 2015, **27**, 1255-1261.
122. J. Li, M. Hu, H. Pei, X. Ma, F. Yan, D. S. Dlamini, Z. Cui, B. He, J. Li and H. Matsuyama, *J. Membr. Sci.*, 2020, **595**, 117547.
123. Y. Mo, X. Zhao and Y. Shen, *Desalination*, 2016, **399**, 40-46.
124. F. Baskoro, C. Wong, S. R. Kumar, C. Chang, C. Chen, D. W. Chen and S. J. Lue, *J. Membr. Sci.*, 2018, **554**, 253-263.
125. T. Liu, B. Yang, N. Graham, W. Yu and K. Sun, *J. Membr. Sci.*, 2017, **542**, 31-40.
126. Y. Du, X. Zhang, J. Yang, Y. Lv, C. Zhang and Z. K. Xu, *J. Membr. Sci.*, 2020, **595**, 117586.
127. Y. Ma, Y. Su, M. He, B. Shi, R. Zhang, J. Shen and Z. Jiang, *ACS Appl. Mater. Interfaces*, 2018, **10**, 37489-37497.
128. S. Wang, D. Mahalingam, B. Sutisna and S. P. Nunes, *J. Mater. Chem. A*, 2019, **7**, 11673-11682.
129. R. Han and P. Wu, *J. Mater. Chem. A*, 2019, **7**, 6475-6481.
130. W. Li, Y. Zhang, P. Su, Z. Xu, G. Zhang, C. Shen and Q. Meng, *J. Mater. Chem. A*, 2016, **4**, 18747-18752.
131. M. Zhang, K. Guan, J. Shen, G. Liu, Y. Fan and W. Jin, *AIChE J.*, 2017, **63**, 5054-5063.
132. D. V. Lam, T. Gong, S. Won, J. Kim, H. Lee, C. Lee and S. Lee, *Chem. Commun.*, 2015, **51**, 2671-2674.
133. P. Su, W. Li, C. Zhang, Q. Meng, C. Shen and G. Zhang, *J. Mater. Chem. A*, 2015, **3**, 20345-20351.
134. W. Li, Y. Zhang, Z. Xu, Q. Meng, Z. Fan, S. Ye and G. Zhang, *Angew. Chem. Int. Ed.*, 2016, **55**, 955-959.
135. C. Zhang, B. Wu, M. Ma, Z. Wang and Z. Xu, *Chem. Soc. Rev.*, 2019, **48**, 3811-3841.
136. W. Li, J. Shi, Z. Li, W. Wu, Y. Xia, Y. Yu and G. Zhang, *Adv. Mater. Interfaces*, 2018, **5**, 1800032.
137. H. Yang, N. Wang, L. Wang, H. Liu, Q. An and S. Ji, *J. Membr. Sci.*, 2018, **545**, 158-166.
138. X. Wang, L. Chen, S. Y. Chong, M. A. Little, Y. Wu, W. Zhu, R. Clowes, Y. Yan, M. A. Zwijnenburg, R. S. Sprick and A. I. Cooper, *Nat. Chem.*, 2018, **10**, 1180-1189.
139. Y. Liu, J. Guan, Y. Su, R. Zhang, J. Cao, M. He, J. Yuan, F. Wang, X. You and Z. Jiang, *J. Mater. Chem. A*, 2019, **7**, 25458-25466.
140. X. Zhang, H. Li, J. Wang, D. Peng, J. Liu and Y. Zhang, *J. Membr. Sci.*, 2019, **581**, 321-330.
141. S. J. Gao, H. Qin, P. Liu and J. Jin, *J. Mater. Chem. A*, 2015, **3**, 6649-6654.
142. W. Hung, T. Lin, Y. Chiao, A. Sengupta, Y. Hsiao, S. R. Wickramasinghe, C. Hu, K. Lee and J. Lai, *J. Mater. Chem. A*, 2018, **6**, 19445-19454.

143. T. Yang, H. Lin, K. P. Loh and B. Jia, *Chem. Mater.*, 2019, **31**, 1829-1846.
144. M. Kunimatsu, K. Nakagawa, T. Yoshioka, T. Shintani, T. Yasui, E. Kamio, S. C. E. Tsang, J. Li and H. Matsuyama, *J. Membr. Sci.*, 2020, **595**, 117598.
145. W. Wang, E. Eftekhari, G. Zhu, X. Zhang, Z. Yan and Q. Li, *Chem. Commun.*, 2014, **50**, 13089-13092.
146. G. Zhao, R. Hu, X. Zhao, Y. He and H. Zhu, *J. Membr. Sci.*, 2019, **585**, 29-37.
147. N. Padmavathy, S. S. Behera, S. Pathan, L. Das Ghosh and S. Bose, *ACS Appl. Mater. Interfaces*, 2019, **11**, 7566-7575.
148. Y. Han, Y. Jiang and C. Gao, *ACS Appl. Mater. Interfaces*, 2015, **7**, 8147-8155.
149. K. Goh, W. Jiang, H. E. Karahan, S. Zhai, L. Wei, D. Yu, A. G. Fane, R. Wang and Y. Chen, *Adv. Funct. Mater.*, 2015, **25**, 7348-7359.
150. M. Musielak, A. Gagor, B. Zawisza, E. Talik and R. Sitko, *ACS Appl. Mater. Interfaces*, 2019, **11**, 28582-28590.
151. L. Liu, Y. Zhou, J. Xue and H. Wang, *AIChE J.*, 2019, **65**, e16699.
152. Y. H. Xi, J. Q. Hu, Z. Liu, R. Xie, X. J. Ju, W. Wang and L. Y. Chu, *ACS Appl. Mater. Interfaces*, 2016, **8**, 15557-15566.
153. G. Kong, J. Pang, Y. Tang, L. Fan, H. Sun, R. Wang, S. Feng, Y. Feng, W. Fan, W. Kang, H. Guo, Z. Kang and D. Sun, *J. Mater. Chem. A*, 2019, **7**, 24301-24310.
154. N. A. Khan, J. Yuan, H. Wu, L. Cao, R. Zhang, Y. Liu, L. Li, A. U. Rahman, R. Kasher and Z. Jiang, *ACS Appl. Mater. Interfaces*, 2019, **11**, 28978-28986.
155. J. Sun, H. Bi, S. Su, H. Jia, X. Xie and L. Sun, *J. Membr. Sci.*, 2018, **553**, 131-138.
156. L. Chen, N. Li, Z. Wen, L. Zhang, Q. Chen, L. Chen, P. Si, J. Feng, Y. Li, J. Lou and L. Ci, *Chem. Eng. J.*, 2018, **347**, 12-18.
157. H. Huang, Z. Song, N. Wei, L. Shi, Y. Mao, Y. Ying, L. Sun, Z. Xu and X. Peng, *Nat. Commun.*, 2013, **4**, 2979.
158. Y. Zhan, S. He, X. Wan, S. Zhao and Y. Bai, *J. Membr. Sci.*, 2018, **567**, 76-88.
159. S. Wei, Y. Xie, Y. Xing, L. Wang, H. Ye, X. Xiong, S. Wang and K. Han, *J. Membr. Sci.*, 2019, **582**, 414-422.
160. P. Cheng, Y. Chen, Y. Gu, X. Yan and W. Lang, *J. Membr. Sci.*, 2019, **591**, 117308.
161. H. Lin, N. Mehra, Y. Li and J. Zhu, *J. Membr. Sci.*, 2020, **593**, 117401.
162. M. Ostwal, D. B. Shinde, X. Wang, I. Gadwal and Z. Lai, *J. Membr. Sci.*, 2018, **550**, 145-154.
163. X. Liu, N. K. Demir, Z. Wu and K. Li, *J. Am. Chem. Soc.*, 2015, **137**, 6999-7002.
164. W. Li, Y. Zhang, C. Zhang, Q. Meng, Z. Xu, P. Su, Q. Li, C. Shen, Z. Fan, L. Qin and G. Zhang, *Nat. Commun.*, 2016, **7**, 11315.
165. X. Li, Y. Liu, J. Wang, J. Gascon, J. Li and B. Van der Bruggen, *Chem. Soc. Rev.*, 2017, **46**, 7124-7144.
166. K. Guan, D. Zhao, M. Zhang, J. Shen, G. Zhou, G. Liu and W. Jin, *J. Membr. Sci.*, 2017, **542**, 41-51.
167. Y. Wei, Y. Zhang, X. Gao, Y. Yuan, B. Su and C. Gao, *Carbon*, 2016, **108**, 568-575.
168. K. G. Zhou, K. S. Vasu, C. T. Cherian, M. Neek-Amal, J. C. Zhang, H. Ghorbanfekr-Kalashami, K. Huang, O. P. Marshall, V. G. Kravets, J. Abraham, Y. Su, A. N. Grigorenko, A. Pratt, A. K. Geim, F. M. Peeters, K. S. Novoselov and R. R. Nair, *Nature*, 2018, **559**, 236-240.
169. C. Cheng, G. Jiang, G. P. Simon, J. Z. Liu and D. Li, *Nat. Nanotechnol.*, 2018, **13**, 685-690.
170. S. P. Surwade, S. Chai, J. Choi, X. Wang, J. S. Lee, I. V. Vlassiouk, S. M. Mahurin and S. Dai, *Langmuir*, 2014, **30**, 3606-3611.
171. D. Cohen-Tanugi and J. C. Grossman, *Nano Lett.*, 2012, **12**, 3602-3608.
172. S. P. Surwade, S. N. Smirnov, I. V. Vlassiouk, R. R. Unocic, G. M. Veith, S. Dai and S. M. Mahurin, *Nat. Nanotechnol.*, 2015, **10**, 459-464.
173. L. Mao, H. Park, R. A. Soler-Crespo, H. D. Espinosa, T. H. Han, S. T. Nguyen and J. Huang, *Nat. Commun.*, 2019, **10**, 3677.
174. Y. Ying, L. Sun, Q. Wang, Z. Fan and X. Peng, *RSC Adv.*, 2014, **4**, 21425-21428.
175. L. C. Lin and J. C. Grossman, *Nat. Commun.*, 2015, **6**, 8335.
176. Z. Li, X. Zhang, H. Tan, W. Qi, L. Wang, M. C. Ali, H. Zhang, J. Chen, P. Hu, C. Fan and H. Qiu, *Adv. Funct. Mater.*, 2018, **28**, 1805026.
177. S. D. Lacey, D. J. Kirsch, Y. Li, J. T. Morgenstern, B. C. Zarket, Y. Yao, J. Dai, L. Q. Garcia, B. Liu, T. Gao, S. Xu, S. R. Raghavan, J. W. Connell, Y. Lin and L. Hu, *Adv. Mater.*, 2018, **30**, 1705651.
178. S. C. O'Hern, D. Jang, S. Bose, J. C. Idrobo, Y. Song, T. Laoui, J. Kong and R. Karnik, *Nano Lett.*, 2015, **15**, 3254-3260.
179. P. R. Kidambi, D. Jang, J. Idrobo, M. S. H. Boutilier, L. Wang, J. Kong and R. Karnik, *Adv. Mater.*, 2017, **29**, 1700277.
180. J. Shi, W. Wu, Y. Xia, Z. Li and W. Li, *Desalination*, 2018, **441**, 77-86.
181. P. Sun, M. Zhu, K. Wang, M. Zhong, J. Wei, D. Wu, Z. Xu and H. Zhu, *ACS Nano*, 2013, **7**, 428-437.
182. R. K. Joshi, P. Carbone, F. C. Wang, V. G. Kravets, Y. Su, I. V. Grigorieva, H. A. Wu, A. K. Geim and R. R. Nair, *Science*, 2014, **343**, 752-754.
183. J. Yang, X. Hu, X. Kong, P. Jia, D. Ji, D. Quan, L. Wang, Q. Wen, D. Lu, J. Wu, L. Jiang and W. Guo, *Nat. Commun.*, 2019, **10**, 1171.
184. N. Aba, J. Chong, B. Wang, C. Mattevi and K. Li, *J. Membr. Sci.*, 2015, **484**, 87-94.
185. J. Liu, N. Wang, L. J. Yu, A. Karton, W. Li, W. Zhang, F. Guo, L. Hou, Q. Cheng, L. Jiang, D. A. Weitz and Y. Zhao, *Nat. Commun.*, 2017, **8**, 2011.
186. J. Liu, L. Yu, G. Yue, N. Wang, Z. Cui, L. Hou, J. Li, Q. Li, A. Karton, Q. Cheng, L. Jiang and Y. Zhao, *Adv. Funct. Mater.*, 2019, **29**, 1808501.
187. L. Dong, W. Fan, X. Tong, H. Zhang, M. Chen and Y. Zhao, *J. Mater. Chem. A*, 2018, **6**, 6785-6791.
188. L. Huang, Y. Li, Q. Zhou, W. Yuan and G. Shi, *Adv. Mater.*, 2015, **27**, 3797-3802.
189. X. Lin, X. Shen, Q. Zheng, N. Yousefi, L. Ye, Y. Mai and J. Kim, *ACS Nano*, 2012, **6**, 10708-10719.
190. L. Huang, J. Chen, T. Gao, M. Zhang, Y. Li, L. Dai, L. Qu and G. Shi, *Adv. Mater.*, 2016, **28**, 8669-8674.
191. M. Ang, M. Gallardo, G. Dizon, M. De Guzman, L. Tayo, S. Huang, C. Lai, H. Tsai, W. Hung, C. Hu, Y. Chang and K. Lee, *J. Membr. Sci.*, 2019, **587**, 117188.
192. F. Liang, Q. Liu, J. Zhao, K. Guan, Y. Mao, G. Liu, X. Gu and W. Jin, *AIChE J.*, 2020, **66**, e16812.

This review concludes and discusses the remarkable progresses of GO membranes, especially the strategies and mechanisms for controlling their transport pathways in liquid separation.